Journal of Nuclear Medicine, published on March 8, 2019 as doi:10.2967/jnumed.118.224469

Development of novel FAP-targeted radiotracers with improved tumor retention

Anastasia Loktev[1,2], Thomas Lindner[1], Eva-Maria Burger[1], Annette Altmann[1,2], Frederik Giesel[1], Clemens Kratochwil[1], Jürgen Debus[3,4], Frederik Marmé[5], Dirk Jäger[6], Walter Mier[1], Uwe Haberkorn [1,2,7§]

(1) Department of Nuclear Medicine, University Hospital Heidelberg, Heidelberg Germany.

(2) Clinical Cooperation Unit Nuclear Medicine, German Cancer Research Center (DKFZ), Heidelberg, Germany.

(3) Dept. of Radiation Oncology, University Hospital Heidelberg, Heidelberg, Germany

(4) Clinical Cooperation Unit Radiation Oncology, German Cancer Research Center (DKFZ), Heidelberg, Germany

(5) Department of Gynecologic Oncology, National Center for Tumor Diseases (NCT) and Department of Obstetrics and Gynecology, University Women's Clinic, University Hospital Heidelberg, Germany

(6) Dept. of Medical Oncology, National Center for Tumor Diseases (NCT), Heidelberg, Germany

(7) Translational Lung Research Center Heidelberg (TLRC), German Center for Lung Research (DZL), Heidelberg, Germany

[§]Corresponding author:

Uwe Haberkorn

Department of Nuclear Medicine

University Hospital Heidelberg

Im Neuenheimer Feld 400

69120 Heidelberg

Tel: +49-6221-56-7732

Fax: +49-6221-56-5473

Email: Uwe.Haberkorn@med.uni-heidelberg.de

First author:

Anastasia Loktev

Department of Nuclear Medicine

University Hospital Heidelberg

Im Neuenheimer Feld 400

69120 Heidelberg

Tel: +49-6221-56-7571

Email: Anastasia.Loktev@med.uni-heidelberg.de

Conflicts of interest: Patent application (EP 18155420.5) for quinolone based FAP targeting agents for imaging and therapy in nuclear medicine (UH, AL, TL, CK, FG and WM).

Keywords: Fibroblast activation protein, PET/CT, theranostics, FAP inhibitor, tracer development

Word count: 4455

ABSTRACT

Purpose: Cancer associated fibroblasts constitute a vital subpopulation of the tumor stroma and are present in more than 90% of epithelial carcinomas. The overexpression of the serine protease fibroblast activation protein (FAP) allows a selective targeting of a variety of tumors by inhibitor-based radiopharmaceuticals (FAPIs). Of these compounds, FAPI-04 has been recently introduced as theranostic radiotracer and demonstrated high uptake into different FAP-positive tumors in cancer patients. To enable the delivery of higher doses, thereby improving the outcome of a therapeutic application, several FAPI variants were designed to further increase tumor uptake and retention of these tracers.

Methods: Novel quinoline-based radiotracers were synthesized by organic chemistry and evaluated in radioligand binding assays using FAP-expressing HT-1080 cells. Depending on their *in vitro* performance, small animal PET imaging and biodistribution studies were performed in HT-1080-FAP tumor bearing mice. The most promising compounds were used for clinical PET imaging in a total of 8 cancer patients.

Results: Compared to FAPI-04, 11 out of 15 FAPI derivatives showed improved FAP binding *in vitro*. Of these, 7 compounds demonstrated increased tumor uptake in tumor bearing mice. Moreover, tumor-to-normal organ ratios were improved for a majority of the compounds, resulting in images with higher contrast. Notably two of the novel radiotracers, FAPI-21 and -46, displayed substantially improved ratios of tumor to blood, liver, muscle, and intestinal uptake. A first diagnostic application in cancer patients revealed high intratumoral uptake of both radiotracers already ten minutes after administration, but a higher uptake in oral mucosa, salivary glands and thyroid for FAPI-21.

Conclusion: Chemical modification of the FAPI framework enabled enhanced FAP-binding and improved pharmacokinetics in the majority of the derivatives, resulting in high contrast images. Moreover, higher doses of radioactivity can be delivered while minimizing damage of healthy tissue, which may improve therapeutic outcome.

INTRODUCTION

Fibroblast activation protein (FAP), a member of the serine protease family, is expressed in the microenvironment of more than 90% of epithelial tumors, including pancreas, colon, breast and HNO carcinomas(*1*). Despite its controversial pathophysiological role in tumor progression, overexpression of the membrane protein is associated with a poor prognosis and a fast progression of disease(*2-4*). On this account, FAP indisputably represents an interesting target structure for imaging and the targeted delivery of therapeutically active compounds (*1,5-9*). In our previous work, we presented the development of several quinoline-based theranostic radiotracers, which were successfully used for tumor imaging of a multitude of different cancers, including pancreas, breast and colon carcinoma as well as high-grade glioblastoma(*10,11*).

Originating from the initial lead structure FAPI-02, a first improvement with regard to tumor retention was already obtained by chemical modification of the molecule. While the tumor uptake from 1 to 3 h p.i. decreased by 75 % for FAPI-02, tumor retention was slightly prolonged with FAPI-04 (50 % washout). A comparison with the commonly used radiotracer ^{18}F-FDG revealed equal or improved tumor-to-background contrast ratios for FAPI-04 in a total of six cancer patients(*12*). Moreover, a first therapeutic approach using beta-emitting radionuclides was adopted, proving safety and harmlessness of the novel pharmaceuticals. Efficient endoradiotherapeutic use of the FAPI tracers, however, is still limited due to their relatively short tumor retention time. We therefore aimed for further development of these FAP-targeting molecules to increase the total tumor dose while maintaining low unspecific binding to healthy tissue.

MATERIALS AND METHODS

Chemistry

All solvents and non-radioactive reagents (except for solid phase peptide synthesis) were obtained in reagent grade from ABCR (Karlsruhe, Germany), Sigma-Aldrich (München, Germany), Acros Organics (Geel, Belgium) or VWR (Bruchsal, Germany) and were used without further purification. All FAPI-derivatives up to FAPI-36 were synthesized as previously described(*10,11*), while the attachment of the bicyclic diamines required higher temperatures and longer reaction times. The triazole ring of FAPI-37 was formed by copper catalysed Huisgen reaction of an azide substituted quinoline-4-carboxylic acid with propargylamine. For FAPI-39, -40, -41 as well as -46, -53 and -55 a palladium catalysed coupling reaction was performed with *tert*-butyl 6-bromoquinoline-4-carboxylate and the individual linker reagent. For more detailed information on compound chemistry and synthesis see supplemental information.

Radiolabeling

^{177}Lu and ^{68}Ga were chelated after pH adjustment with sodium acetate. The reaction mixture was heated to 95 °C for 10 min and completeness of reaction was checked by radio-HPLC. ^{177}Lu labeled FAPIs were used directly for *in vitro* studies or diluted with 0.9% saline and directly applied for organ distribution studies. The ^{68}Ga compounds were processed by solid phase extraction prior to PET-imaging.

Cell culture

HT-1080 cells transfected with the human FAP-gene as well as murine FAP and CD26 transfected human embryonic kidney cells (obtained from Stefan Bauer, NCT Heidelberg(*13*)) were cultivated in Dulbecco's modified Eagle's medium (DMEM) containing 10% fetal calf serum at 37°C/5% carbon dioxide.

For radioligand binding studies, cells were seeded in 6-well plates and cultivated for 48 h to a final confluence of approx. 80 - 90% (1.2 - 2 mio cells/well). The medium was replaced by 1 mL fresh medium without fetal calf serum. The radiolabeled compound was added to the cell culture and incubated for different time intervals ranging from 10 min to 24 h. Competition experiments were

performed by simultaneous exposure to unlabeled (10^{-5} M to 10^{-10} M) and radiolabeled compound for 60 min. Cell efflux was determined after incubation of the cells with the tracer for 60 minutes. Thereafter, the radioactive medium was removed, cells were washed and incubated with nonradioactive medium for 1, 2, 4 and 24 hours. In all experiments, the cells were washed twice with 1 mL phosphate-buffered saline pH 7.4 and subsequently lysed with 1.4 ml lysis buffer (0.3 M NaOH, 0.2% SDS). Radioactivity was determined in a γ-counter (Cobra II, Packard), normalized to 1 mio cells and calculated as percentage of the applied dose (%AD). Each experiment was performed 3 times, and 3 repetitions per independent experiment were acquired.

Animal studies

For *in vivo* experiments, 8-week-old BALB/c nu/nu mice (Charles River) were subcutaneously inoculated into the right trunk with 5 mio HT-1080-FAP cells. When the size of the tumor reached approximately 1 cm^3, the radiolabeled compound was injected via the tail vein (80 nmol/GBq for small-animal PET imaging; 200 nmol/GBq for organ distribution). *In vivo* blocking experiments were performed by adding 30 nmol unlabeled FAPI to the radiolabeled compound directly prior to injection. For organ distribution, the animals (n = 3 for each time point) were sacrificed 1, 4, 6 and 24 after tracer administration. The distributed radioactivity was measured in all dissected organs and in blood using a γ-counter (Cobra Autogamma, Packard). The values are expressed as percentage of injected dose per gram of tissue (%ID/g). PET imaging was performed using a small-animal PET scanner (Inveon, Siemens). Within the first 60 min a dynamic scan was performed in list mode, followed by a static scan from 120 to 140 min after injection. Images were reconstructed iteratively using the 3D-OSEM+MAP method (Siemens) and were converted to standardized uptake value (SUV) images. For the dynamic data 28 frames were reconstructed: 4 x 5 sec, 4 x 10 sec, 4 x 20 sec, 4 x 60 sec, 4 x 120 sec, 6 x 300 sec and 2 x 470 sec. Quantification was done using a ROI technique and expressed as SUV. All animal experiments

were conducted in compliance with the German animal protection laws (permission number 35-91185.81/G-158/15).

Statistical analysis

Statistical analysis of the cell culture and animal experiments was performed using GraphPad Prism 7.0 (GraphPad Software, San Diego, USA). Unless stated otherwise, all values are expressed as mean ± standard deviation (SD). For normal distributed populations, comparisons between means of different groups were performed using an unpaired t-test.

Clinical PET/CT-imaging

Imaging of 8 patients was performed under the conditions of the updated declaration of Helsinki, § 37 (unproven interventions in clinical practice) and in accordance to the German Pharmaceuticals Law §13 (2b) for medical reasons using ^{68}Ga-FAPI-21 and -46, which was applied intravenously (20 nmol, 210-267 MBq for FAPI-21 and 216-242 MBq for FAPI-46), 10 min, 1 and 3 hours post tracer administration. The PET/CT scans were performed with a Biograph mCT Flow™ PET/CT-Scanner (Siemens Medical Solutions) using the following parameters: slice thickness of 5 mm, increment of 3-4 mm, soft-tissue reconstruction kernel, care dose. Immediately after CT scanning, a whole-body PET was acquired in 3D (matrix 200x200) in FlowMotion™ with 0.7 cm/min. The emission data were corrected for random, scatter and decay. Reconstruction was conducted with an ordered subset expectation maximisation (OSEM) algorithm with 2 iterations/21 subsets and Gauss-filtered to a transaxial resolution of 5 mm at full-width half-maximum (FWHM). Attenuation correction was performed using the low-dose non-enhanced CT data. The quantitative assessment of standardized uptake values (SUV) was done using a region of interest technique. The data were analyzed retrospectively with approval of the local ethics committee (No. S016/2018).

RESULTS

Chemical modification of the FAPI framework results in increased FAP-binding *in vitro*

To determine the FAP binding affinities of the novel radiotracers (Suppl. Table 1), radioligand binding assays were performed using human FAP-expressing HT-1080 cells. To compensate for varying rates of FAP-expression and allow a direct comparison with the lead structure, all experiments were conducted in parallel with FAPI-04. All compounds demonstrated robust binding to human FAP with binding values equal to or higher than FAPI-04 after 1 and 4 h of incubation (Figure 1). Internalization rates were comparable to those of FAPI-04 for all compounds, except for FAPI-38 (63.1 % internalized after 24 h, FAPI-04: 97.1 %; see Suppl. Table 2). While most of the derivatives revealed higher binding values after 24 h as compared to FAPI-04, the compounds FAPI-38, -39, -40 and -41 were eliminated significantly faster from FAP-expressing cells and were, therefore, not considered for a more detailed characterization. Similar to FAPI-04, all compounds demonstrated negligibly low binding to the structurally related membrane protein CD26 (data not shown).

Improvement of pharmacokinetics and image contrast for positron emission tomography

In order to assess a potential increase in tumor retention and to evaluate their pharmacokinetic behavior, the most promising candidates were analyzed *in vivo*. To this end, small animal PET imaging was performed in HT-1080-FAP xenografted mice. All compounds demonstrated rapid tumor accumulation with overall low background activity and predominant renal elimination (Suppl. Fig. 4). Highest tumor uptake was observed for FAPI-55 (SUV max 1.8 after 60 min, 1.7 after 120 min), followed by FAPI-36 (1.5 after 60 min, 1.3 after 120 min) and FAPI-21 (1.3 after 60 and 120 min) (Figure 2, Suppl. Fig. 5). As the absolute uptake values allow only limited comparison of the radiotracers, AUC values were calculated from the time-activity curves, representing the accumulated radioactivity within the time interval up to 2 h after injection. As shown in Table 1, seven out of ten compounds demonstrated higher tumor uptake values as compared to FAPI-04, headed by FAPI-21, -36, -46 and -55. Yet, FAPI-36 showed a prolonged systemic circulation, resulting in unfavorable tumor-to-blood ratios and a poorer image

contrast as compared to FAPI-04 (Suppl. Fig. 4). While the tumor-to-blood and tumor-to-liver ratios for FAPI-35 were comparable to those of FAPI-04, tumor-to-muscle ratio was slightly improved (Figure 3). FAPI-21 and -55 demonstrated higher accumulation in liver and muscle tissue as compared to FAPI-04. From all tested compounds, FAPI-46 displayed the highest tumor-to-blood, tumor-to-muscle and tumor-to-liver ratios.

Based on the observations of the imaging studies, FAPI-21, -35, -46 and -55 were selected for a more detailed characterization in biodistribution studies using ^{177}Lu-labeled radiotracers. As shown in Figure 4, all compounds demonstrated robust tumor accumulation with overall low uptake into healthy tissue. Moderate radioactivity (1.8 - 3.5 %ID/g 1 h after injection) was measured merely in the kidneys, due to predominant renal elimination of the radiotracers with activity mostly in the renal calyx system. In comparison to FAPI-04, FAPI-21 and -46 demonstrated higher tumor accumulation 1 and 4 h after injection. While all other compounds displayed their highest intratumoral radioactivity 1 h after injection, tumor uptake was even increasing from 1 to 4 h for FAPI-21. In addition, FAPI-21 revealed the highest tumor retention 24 h after injection (6.03 ± 0.68 %ID/g), followed by FAPI-35 (2.47 ± 0.23 %ID/g) and -46 (2.29 ± 0.16 %ID/g), featuring similar uptake rates as FAPI-04 (2.86 ± 0.31 %ID/g). Accordingly, 64% of the maximum tumor activity were still present 24 h after injection for FAPI-21, followed by FAPI-35 (37%), FAPI-46 and -55 (almost 20% each). In comparison to FAPI-04, radioactivity levels in the blood were equal or marginally higher at all specified times, except for FAPI-55, which demonstrated the highest blood activities of all compounds up to 6 h after injection. However, blood activity was decreasing steadily, reaching similar values as FAPI-04 after 24 h. All derivatives demonstrated an increased liver uptake as compared to FAPI-04, except for FAPI-46, which displayed comparable activities up to 6 h after injection, but narrowed to lower levels in the course of 24 h. Renal activity of the compounds was comparable for FAPI-04, -21 and -35 but significantly reduced for FAPI-46 and -55 at all specified times. A comparison of AUC values, determined from the time-activity curves from 1 to 24 h after injection, revealed the highest overall tumor uptake for FAPI-21, followed by FAPI-46 (Table 2). A

calculation of tumor-to-organ ratios, based on the overall AUC values, evinced a general improvement of pharmacokinetics for FAPI-21 and -46 and no considerable change for all the other radiotracers, except for FAPI-35 (Figure 5, Suppl. Table 3). Notably FAPI-46 displayed substantially improved ratios of tumor to liver, renal and brain uptake.

FAPI-21 and -46 highly accumulate in various tumors in humans

Whole body PET/CT scans were performed 10 min, 1 and 3 h after intravenous administration of ^{68}Ga-FAPI-21 or -46 in patients with metastasized mucoepidermoid, oropharynx, ovarial and colorectal carcinoma. Both radiotracers rapidly accumulated in the primary tumors and the metastases, with maximum SUV values of 11.9 ± 3.33 for FAPI-21 and 12.76 ± 0.90 for FAPI-46 1 h after administration (Figure 6). Additionally, tracer uptake into normal tissue was very low. The radioactivity was cleared steadily from the blood stream and excreted predominantly via the kidneys, resulting in high contrast images. Interestingly, FAPI-21 demonstrated an increased accumulation in the oral mucosa (SUV max 3.38 ± 1.20; FAPI-46 1.49 ± 1.10), the thyroid (SUV max 3.25 ± 0.89; FAPI-46 2.25 ± 0.46) and the salivary glands (SUV max parotis 3.69 ± 0.89; FAPI-46 1.38 ± 0.26; submandibularis 7.11 ± 1.24; FAPI-46 2.32 ± 0.75).

FAPI-46 demonstrates higher tumor uptake as compared to FAPI-04

In comparison to the lead compound FAPI-04, FAPI-46 displayed higher tumor uptake and comparable activities in healthy tissue (Figure 6G, H). Notably, tumor accumulation rates highly depend on the tumor type. As shown in Table 3, tumor activity of the radiotracers remained relatively constant up to 3 h p.i. in colorectal, ovarian, oropharynx and pancreatic carcinoma whereas a continuous decrease was observed in breast carcinoma. In contrast, tumor accumulation in one patient with carcinoma of unknown primary (CUP) was even increasing from 1 to 3 h after administration (Table 3).

DISCUSSION

The focus of this work was to enhance tumor retention of FAP-targeting radiotracers while simultaneously retaining the excellent imaging contrast of FAPI-02 and FAPI-04, i.e. to develop an optimized theranostic tracer. On this account, 15 novel derivatives were selected and compared to the currently used FAPI-04 with regard to target binding and pharmacokinetic profile. The first approach of derivatization was the alteration of lipophilicity by variations of the linker region, which was chosen for 9 derivatives, mainly bicyclic analogues of the original piperazine moiety. The second approach aimed for modification of the chemistry used for DOTA/linker-attachment at the quinoline moiety. It is based on the effect of the nitrogen atom in the quinoline-4-carboxamide moiety, which accounts for a more than 60-fold reduction of the IC_{50} value compared to an isosteric 1-naphtylcarboxamide based inhibitor(*14*). The rationale was to improve target binding and physicochemical properties by fine-tuning of the electron density at the quinoline moiety by different substituents, which results e.g. in a modified proton acceptor capability. Therefore, the initial ether oxygen was replaced by methylene, sulfur, amino and methylamino moieties. With the intention of achieving synergistic effects, two compounds combining both approaches were additionally synthesized.

A first analysis of the binding properties *in vitro* revealed similar or improved FAP binding of all tested derivatives after 1 and 4 h of incubation as compared to FAPI-04. While most of the compounds demonstrated higher binding values after 24 h, four radiotracers were eliminated significantly faster from FAP-expressing cells. Although the modifications of the piperazine moiety, e.g. the methylene bridged diaminobicycloheptane of FAPI-21, or the linker region, e.g. insertion of the methylamino-group for FAPI-46, had no significant influence on the IC_{50}-values (Suppl. Fig. 3), strong effects on the *in vitro* efflux kinetics were observed (Suppl. Fig. 2). After incubation for 4 h, only 25% of the initial activity of FAPI-04 remained within the cells. In contrast, both FAPI-21 and -46 were eliminated significantly slower from the FAP-expressing cells, with 74% (FAPI-21) and 65% (FAPI-46) of the initial activity being still detectable after 4 h. Although the less degradation-susceptible DOTA-diazabicycloheptane bond may

explain the slower excretion of FAPI-21 as compared to FAPI-04, the longer retention of FAPI-46, which has the same DOTA-piperazine framework as FAPI-04, indicates that the elimination of the cell bound FAPI tracers is an interaction of multiple processes, which are not resolved yet.

Based on the *in vitro* results, 10 out of the initial 15 compounds were selected for PET imaging in FAP-positive tumor bearing mice. Out of these, seven derivatives demonstrated higher tumor uptake values as compared to FAPI-04, headed by FAPI-21, -36, -46 and -55. FAP-specific binding *in vivo* was verified for FAPI-21 and -46 by competition experiments, demonstrating a complete block of tumor accumulation by unlabeled compound (Suppl. Fig. 6). Except for FAPI-35 and -46, all compounds demonstrated significantly higher activities in muscle tissue, which resulted in decreased image contrast. Prolonged systemic circulation, possibly caused by increased albumin binding, was observed for FAPI-36, resulting in unfavorable tumor-to-blood ratios and a poorer image contrast. Moreover, increased blood activities might promote myelotoxic effects and are, therefore, not desirable. FAPI-55, which showed the highest tumor uptake of all compounds, also displayed an increased activity in the liver due to higher lipophilicity. Regarding tumor accumulation, similar results were obtained in a biodistribution study, where FAPI-21, -46 and -55 revealed higher tumor uptake rates as compared to FAPI-04. However, slightly distinct observations were made with regard to liver and renal activity of the compounds as a consequence of altered elimination. As excretory processes are strongly time-dependent, the pharmacokinetic profile within the first two hours after injection appears different from the activities measured at later times up to 24 h after compound administration. While FAPI-55 displayed robust hepatic uptake at early times, liver activity after 24 h was significantly decreased. At the same time, renal accumulation was comparatively low, suggesting a predominant hepatobiliary elimination of the radiotracer. In general, only marginal liver and kidney uptake was observed for all novel derivatives, except for FAPI-35, indicating a rapid body clearance, thus legitimating diagnostic clinical use.

Based on the overall improved tumor-to-normal tissue ratios, FAPI-21 and -46 were chosen for a first diagnostic application in cancer patients. Both compounds demonstrated robust tumor uptake and

overall low background activity. Yet, FAPI-21 displayed an increased uptake in the oral mucosa, the thyroid, the parotid and the submandibular glands for reasons not known yet. This observation, however, represents a major limitation regarding a potential therapeutic application of the tracers. Although the preclinical data suggested a better performance of FAPI-21 compared to FAPI-46, especially with regard to increased tumor uptake, FAPI-46 proved to be more suitable as a theranostic agent in clinical imaging studies due to its lower uptake in normal organs. This observation highlights the diverse nature of human xenotransplants used in mice as compared to tumor metastases in human patients. This may impede a direct translation of results from experimental studies into clinical practice. Unlike in cancer patients, xenograft tumors in mice evolve from a rather homogenous cell population and are characterized by a relatively consistent protein expression. In the animal models used for our experiments, genetically modified FAP-expressing tumor cells were applied, representing a rather artificial tumor model as compared to the clinical situation. Herein, the PET signal is generated by the accumulation of the radiotracers in CAFs evolved from a multitude of different precursor cells, therefore characterized by different protein expression levels. In addition, highest tracer uptake in numerous animal models is often observed in defined tumor areas adjacent to blood vessels, which are well supplied with blood. This allows a rapid accumulation of the radiotracers but a rapid efflux at the same time. In contrast, human tumors form very complex, heterogeneous structures in which perfusion and expression of the target protein may vary significantly. The amount and distribution of FAP-expressing CAFs as well as the number of FAP molecules per cell may differ. This results in different pharmacokinetic profiles of the radiotracers in different tumor types. We observed a different behavior in different types of tumors in this limited cohort of patients: a constant intracellular activity in colorectal, ovarian, oropharynx and pancreatic carcinoma, a continuous decrease in breast carcinoma and an increasing tracer accumulation in one patient with carcinoma of unknown primary (Table 3). A possible explanation might be the heterogeneous origin of CAFs, which may develop from resident fibroblasts, bone marrow derived mesenchymal stem cells, endothelial cells, epithelial cells and even adipocytes (*15-17*). Due to

their difference in origin these CAFs possibly display a different proteome with a strong variation or even lack of FAP expression. Whether this finding of varying kinetics can be extrapolated to these different tumor entities in general has to be determined in a larger number of patients. This type of studies can be expected to reveal important information with respect to the indication of a FAPI-based endoradiotherapy. Tumors with a longer retention of the tracer may respond better than tumors with a fast elimination of the radiopharmaceutical.

CONCLUSION

Based on the lead compound FAPI-04, which is characterized by a rapid uptake into FAP-positive tumors followed by considerable elimination of the tracer, a series of novel derivatives was successfully developed. Notably, the modification of the linker region between the quinoline moiety and the chelator resulted in an increased tumor uptake and improved pharmacokinetic properties of the resulting amino-derivatives, which represent a novel class of radiotracers. Especially FAPI-46 demonstrates improved tumor-to-organ ratios, resulting in an enhanced image contrast for PET imaging. Depending on the tumor type, tumor accumulation could be significantly prolonged by the novel tracer FAPI-46.

ACKNOWLEDGEMENTS

The authors gratefully acknowledge Stefan Bauer (National Center for Tumor Diseases, Heidelberg) for supplying the FAP and CD26 transfected cell lines. The authors thank Christian Kleist, Susanne Krämer, Stephanie Biedenstein, Kirsten Kunze, Irina Kupin, Vanessa Kohl, Marlene Tesch and Karin Leotta for excellent technical assistance. This work was funded in part by the Federal Ministry of Education and Research, grant number 13N 13341.

DISCLOSURE STATEMENT

Patent application for Anastasia Loktev, Thomas Lindner, Walter Mier, Clemens Kratochwil, Frederik Giesel and Uwe Haberkorn. No other potential conflicts of interest relevant to this article exist.

REFERENCES

1. Brennen WN, Isaacs JT, Denmeade SR. Rationale behind targeting fibroblast activation protein-expressing carcinoma-associated fibroblasts as a novel chemotherapeutic strategy. *Mol Cancer Ther.* 2012;11:257-266.

2. Pure E, Blomberg R. Pro-tumorigenic roles of fibroblast activation protein in cancer: back to the basics. *Oncogene.* 2018;37:4343-4357.

3. Busek P, Mateu R, Zubal M, Kotackova L, Sedo A. Targeting fibroblast activation protein in cancer - Prospects and caveats. *Front Biosci (Landmark Ed).* 2018;23:1933-1968.

4. Kilvaer TK, Khanehkenari MR, Hellevik T, et al. Cancer Associated Fibroblasts in Stage I-IIIA NSCLC: Prognostic Impact and Their Correlations with Tumor Molecular Markers. *PLoS One.* 2015;10:e0134965.

5. Loeffler M, Kruger JA, Niethammer AG, Reisfeld RA. Targeting tumor-associated fibroblasts improves cancer chemotherapy by increasing intratumoral drug uptake. *J Clin Invest.* 2006;116:1955-1962.

6. Ostermann E, Garin-Chesa P, Heider KH, et al. Effective immunoconjugate therapy in cancer models targeting a serine protease of tumor fibroblasts. *Clin Cancer Res.* 2008;14:4584-4592.

7. Tanswell P, Garin-Chesa P, Rettig WJ, et al. Population pharmacokinetics of antifibroblast activation protein monoclonal antibody F19 in cancer patients. *Br J Clin Pharmacol.* 2001;51:177-180.

8. Scott AM, Wiseman G, Welt S, et al. A Phase I dose-escalation study of sibrotuzumab in patients with advanced or metastatic fibroblast activation protein-positive cancer. *Clin Cancer Res.* 2003;9:1639-1647.

9. Welt S, Divgi CR, Scott AM, et al. Antibody targeting in metastatic colon cancer: a phase I study of monoclonal antibody F19 against a cell-surface protein of reactive tumor stromal fibroblasts. *J Clin Oncol.* 1994;12:1193-1203.

10. Loktev A, Lindner T, Mier W, et al. A new method for tumor imaging by targeting cancer associated fibroblasts. *J Nucl Med.* 2018.

11. Lindner T, Loktev A, Altmann A, et al. Development of quinoline based theranostic ligands for the targeting of fibroblast activation protein. *J Nucl Med.* 2018.

12. Giesel F, Kratochwil C, Lindner T, et al. FAPI-PET/CT: biodistribution and preliminary dosimetry estimate of two DOTA-containing FAP-targeting agents in patients with various cancers. *J Nucl Med.* 2018.

13. Fischer E, Chaitanya K, Wuest T, et al. Radioimmunotherapy of fibroblast activation protein positive tumors by rapidly internalizing antibodies. *Clin Cancer Res.* 2012;18:6208-6218.

14. Jansen K, Heirbaut L, Cheng JD, et al. Selective Inhibitors of Fibroblast Activation Protein (FAP) with a (4-Quinolinoyl)-glycyl-2-cyanopyrrolidine Scaffold. *ACS Med Chem Lett.* 2013;4:491-496.

15. Kalluri R. The biology and function of fibroblasts in cancer. *Nat Rev Cancer.* 2016;16:582-598.

16. Jacob M, Chang L, Pure E. Fibroblast activation protein in remodeling tissues. *Curr Mol Med.* 2012;12:1220-1243.

17. Cremasco V, Astarita JL, Grauel AL, et al. FAP delineates heterogeneous and functionally divergent stromal cells in immune-excluded breast tumors. *Cancer Immunol Res.* 2018.

	AUC 0-2 h (SUVmean)					Ratios calculated from AUC 0-2h		
	Tumor	Blood	Kidneys	Liver	Muscle	Tu/blood	Tu/muscle	Tu/liver
FAPI-04	58.02	29.54	62.84	19.02	14.57	1.96	3.98	3.05
FAPI-20	57.75	39.71	61.92	30.08	35.56	1.45	1.62	1.92
FAPI-21	**92.59**	40.19	60.01	42.26	20.82	2.30	**4.45**	2.19
FAPI-22	63.95	40.36	42.18	33.99	30.06	1.58	2.13	1.88
FAPI-31	51.76	39.76	48.53	34.32	26.15	1.30	1.98	1.51
FAPI-35	68.11	35.56	47.96	21.83	16.01	1.92	**4.25**	3.12
FAPI-36	**86.74**	75.35	69.92	38.29	19.39	1.15	4.47	2.27
FAPI-37	50.82	41.14	57.38	28.40	34.11	1.24	1.49	1.79
FAPI-46	**79.63**	27.22	39.67	17.82	15.80	**2.93**	**5.04**	**4.47**
FAPI-53	60.85	28.80	52.91	17.40	24.30	2.11	2.50	3.50
FAPI-55	**106.20**	52.78	74.75	42.99	21.81	2.01	**4.87**	2.47

Table 1. AUC values (calculated from SUV mean 0-2 h after intravenous administration) and tumor-to-normal organ ratios for ^{68}Ga-labeled FAPI derivatives. *Tu: tumor.*

	1 h	4 h	6 h	24 h	AUC 1 -24 h
FAPI-04	8.40 ± 0.36	9.44 ± 1.33	7.00 ± 1.20	2.86 ± 0.31	7915
FAPI-21	9.35 ± 1.62	12.38 ± 2.42	12.77 ± 2.88	6.03 ± 0.68	13613
FAPI-35	6.68 ± 1.06	5.35 ± 1.13	5.29 ± 0.51	2.47 ± 0.23	5902
FAPI-46	12.35 ± 6.25	10.60 ± 0.49	8.64 ± 0.52	2.29 ± 0.16	9126
FAPI-55	9.30 ± 2.43	7.53 ± 2.13	7.37 ± 1.32	1.55 ± 0.16	7289

Table 2. Tumor uptake rates of ^{177}Lu-labeled FAPI derivatives (values expressed as %ID/g mean ± SD; n=3) and calculated AUC values.

FAPI-04

	Colorectal Ca.		Colorectal Ca.		Mamma Ca.		Pancreas Ca.	
min	**mean**	**n**	**Mean**	**n**	**mean**	**n**	**mean**	**n**
60	4.77 ± 4.27	3	5.20 ± 0.73	8	3.98 ± 0.80	6	2.90 ± 0.70	3
180	3.67 ± 3.41	3	4.39 ± 1.19	8	3.40 ± 0.78	6	2.90 ± 0.78	3

FAPI-21

	Ovarial Ca.		Ovarial Ca.		Colorectal Ca.		
min	**mean**	**n**	**mean**	**n**	**mean**	**n**	
10	6.41 ± 1.23	3	5.27 ± 1.79	4	5.47 ± 1.83	2	
60	7.48 ± 1.51	3	5.36 ± 1.46	4	4.52 ± 1.22	2	
180	7.42 ± 1.71	3	5.10 ± 1.12	4	3.32 ± 1.06	2	

FAPI-46

	Colorectal Ca.		Mamma Ca.		Oropharynx Ca.		CUP	
min	**mean**	**n**	**mean**	**n**	**mean**	**n**	**mean**	**n**
10	6.85 ± 1.96	4	7.73 ± 1.86	7	6.01 ± 0.82	2	5.41 ± 2.76	4
60	7.23 ± 2.06	4	5.97 ± 0.84	7	6.77 ± 0.65	2	6.45 ± 4.15	4
180	6.40 ± 1.64	4	4.44 ± 0.96	7	6.31 ± 0.25	2	6.93 ± 4.42	4

Table 3. SUV mean values ± standard deviation 10, 60 and 180 min after administration of ^{68}Ga-labeled FAPI-04, -21 and -46 to cancer patients; *n: number of tumor lesions per patient*.

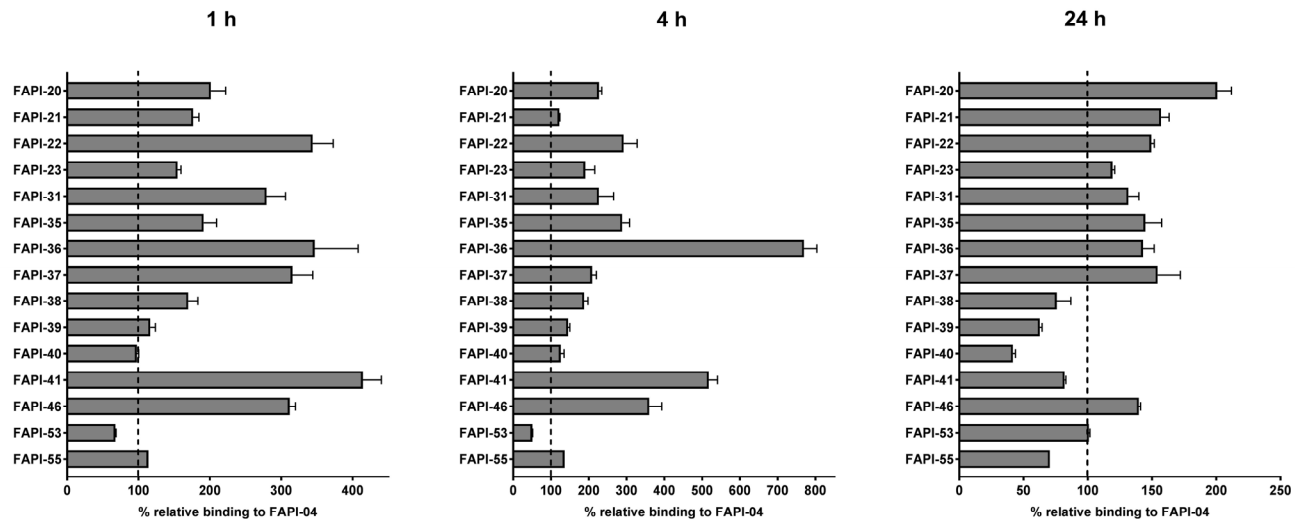

Figure 1. Relative binding rates of ^{177}Lu-labeled FAPI derivatives compared to FAPI-04 (set to 100%) using FAP-expressing HT-1080 cells; n=3.

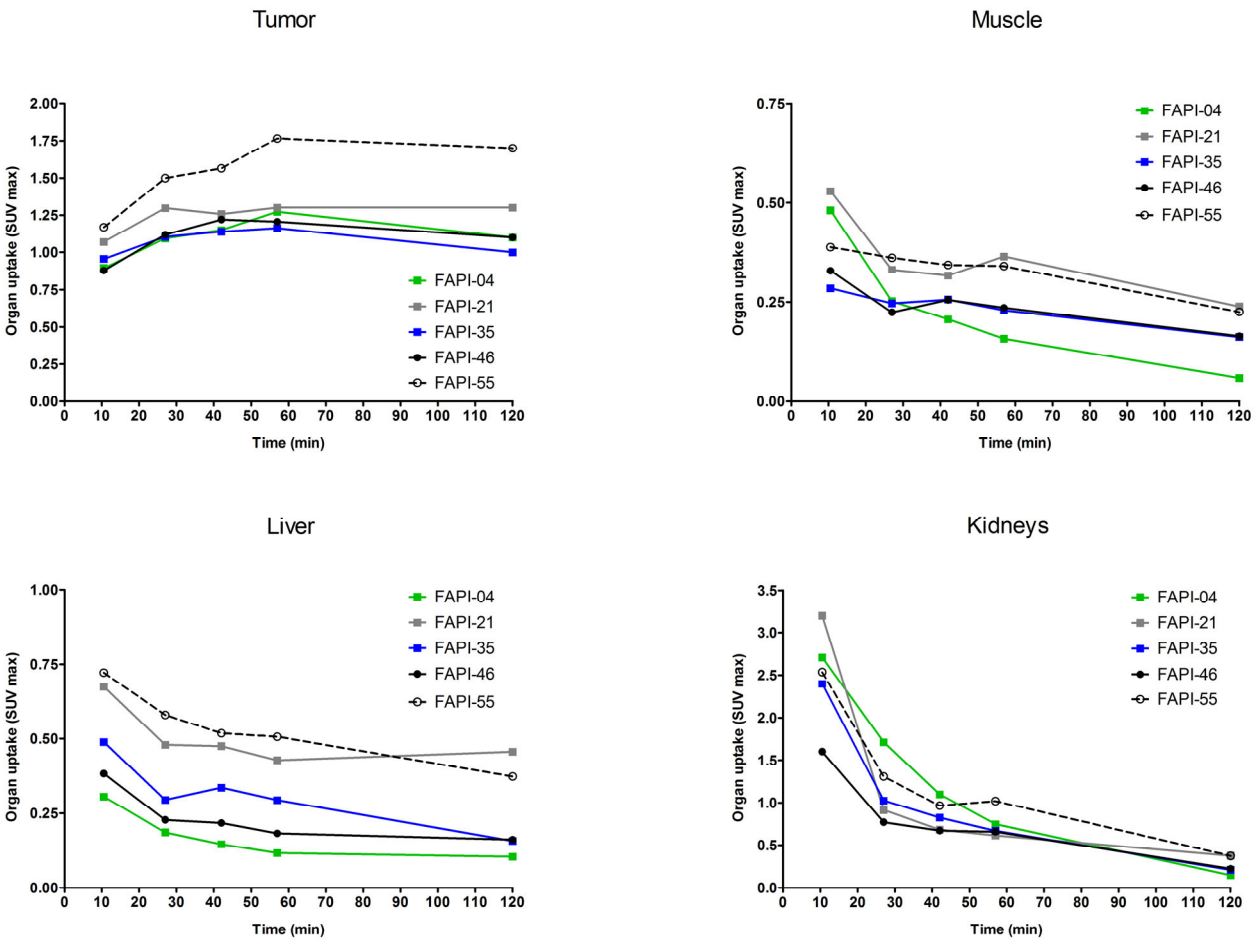

Figure 2. Maximum organ uptake (SUV max) of ^{68}Ga-labeled FAPI derivatives in HT-1080-FAP tumor bearing mice determined by small animal PET imaging; n=1.

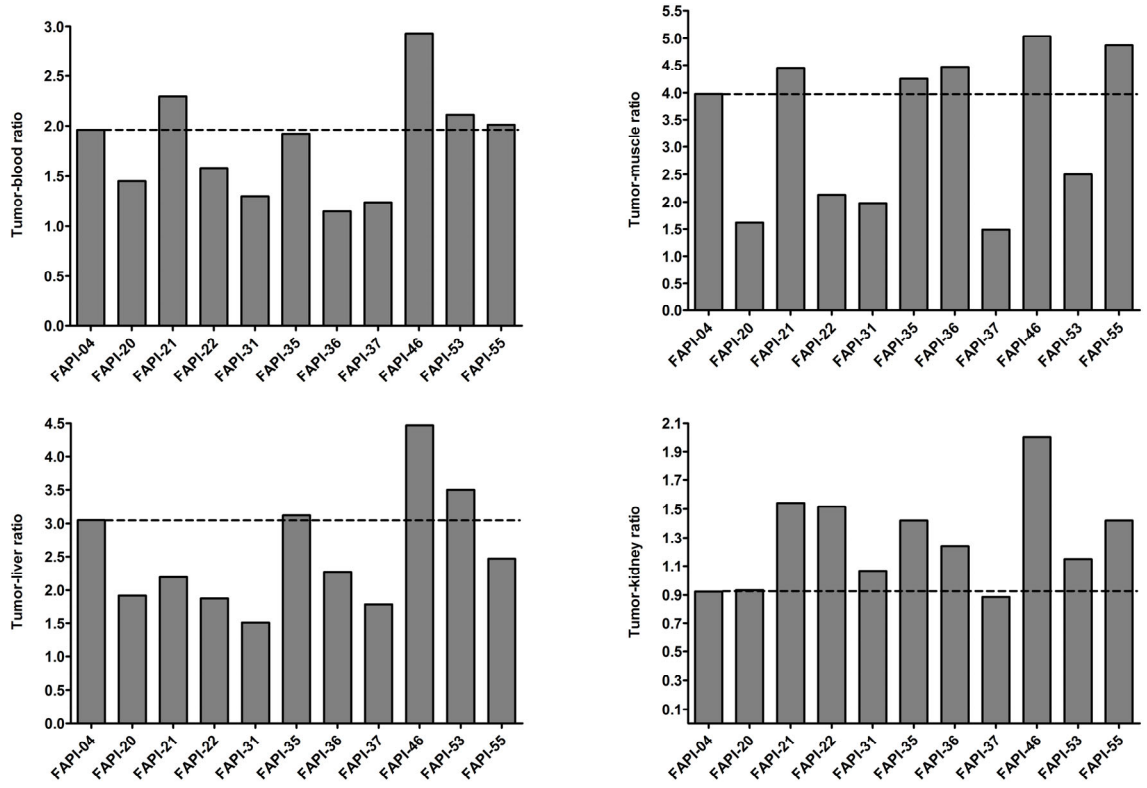

Figure 3. Tumor-to-normal organ ratios of ^{68}Ga-labeled FAPI derivatives, calculated from AUC values 0-2 h after intravenous administration of the radiotracers; n=1.

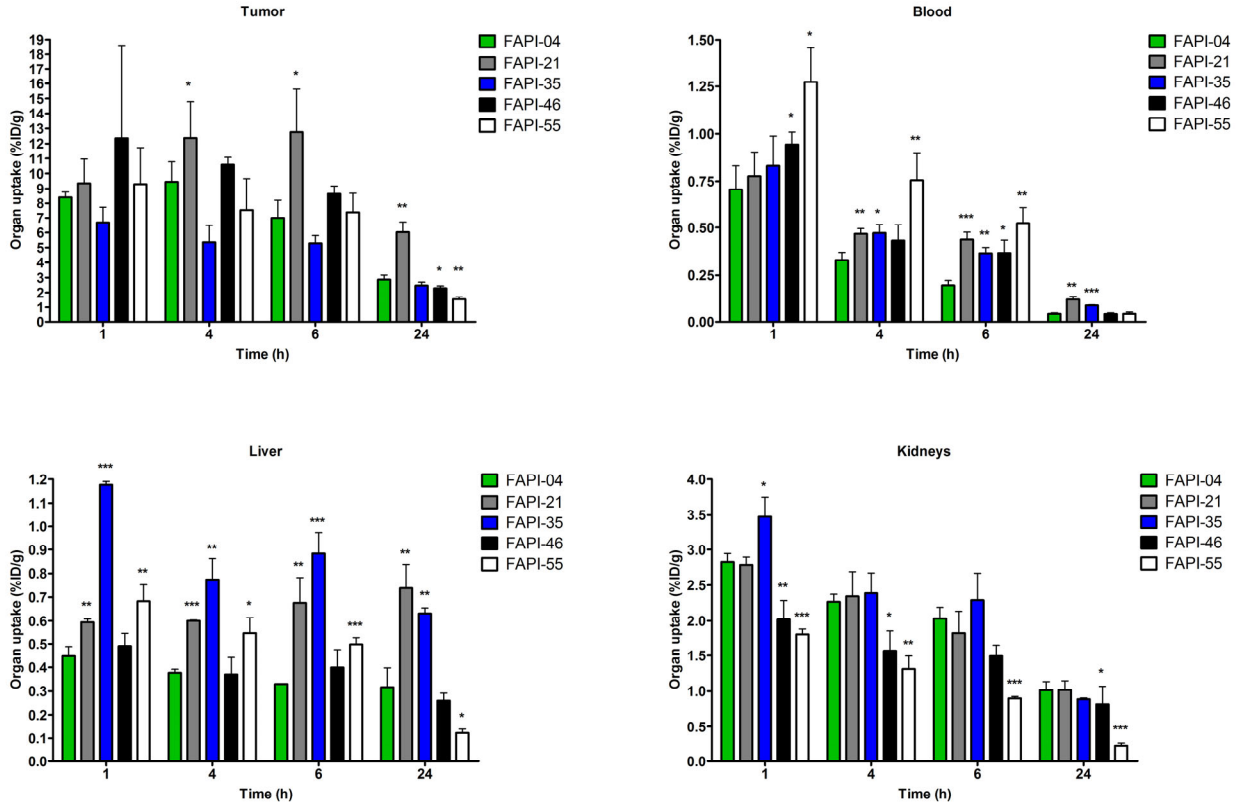

Figure 4. Organ uptake (%ID/g) of ^{177}Lu-labeled FAPI derivatives in HT-1080-FAP tumor bearing mice; n=3; *: p<0.05 **: p<0.01 ***: p<0.001.

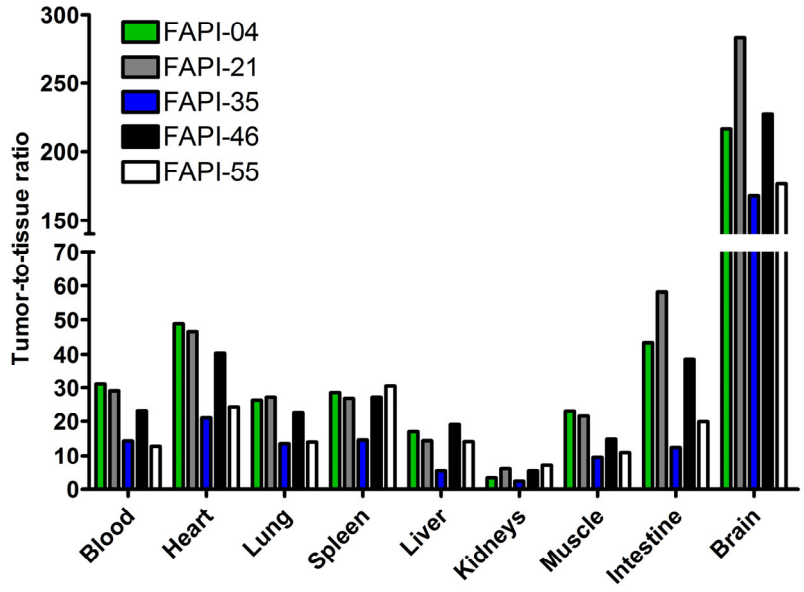

Figure 5. Tumor-to-normal tissue ratios (calculated from %ID/g values 0-24 h after intravenous administration) of ^{177}Lu-labeled FAPI derivatives in HT-1080-FAP tumor bearing mice; n=3.

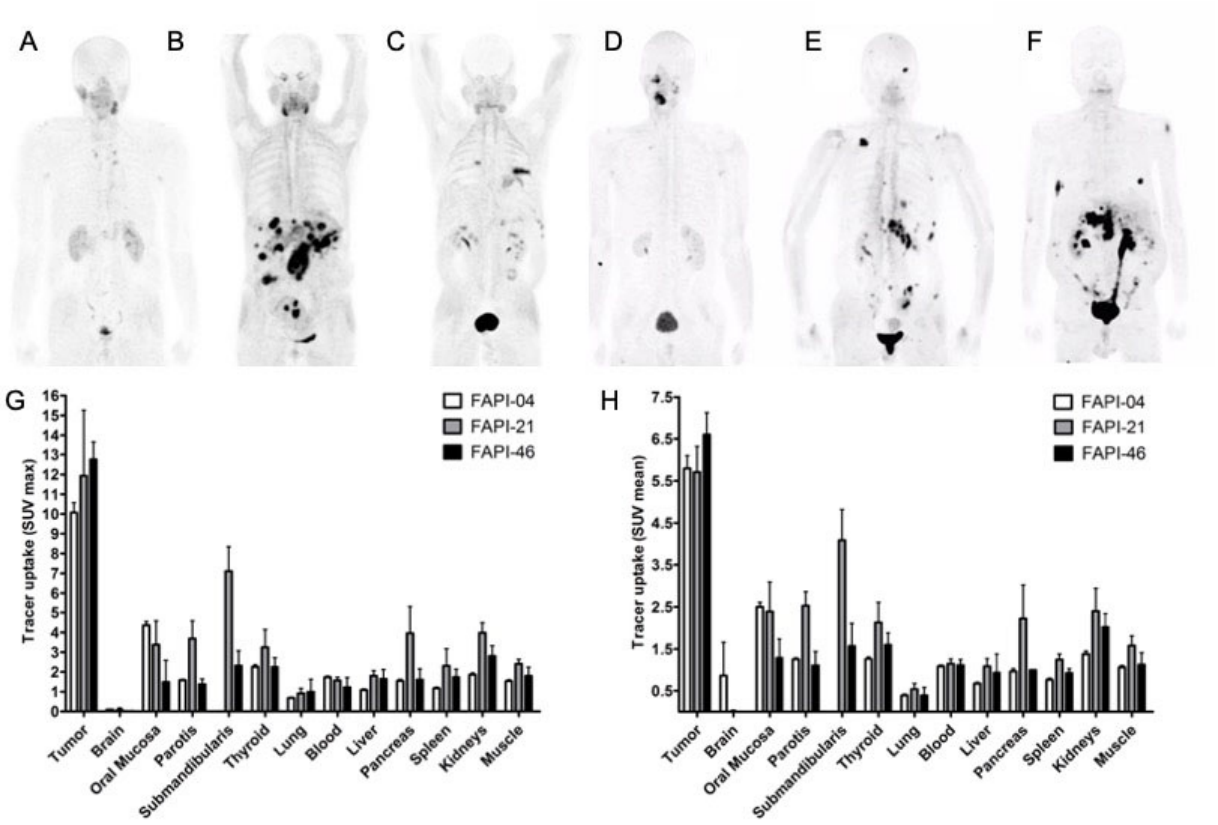

Figure 6. Whole body PET/CT imaging of tumor patients. Maximum intensity projections (MIP) 1 h after intravenous administration of ^{68}Ga-labeled FAPI-21 (A-C) and FAPI-46 (D-F). Maximum (G) and mean (H) tracer uptake of ^{68}Ga-labeled FAPI-21 and -46 in tumor and healthy organs as compared to FAPI-04; n=2-25 (Suppl. Table 4).

Supporting Information

Chemistry

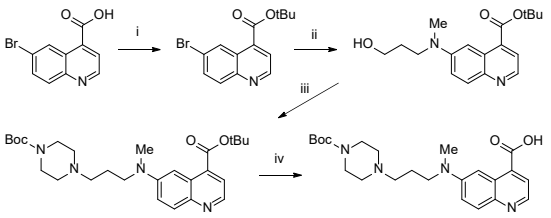

i) DCC, tBuOH, CuCl; ii) $HO(CH_2)_3NHMe$, $Pd_2(dba)_3$, BINAP, Cs_2CO_3; iii) 1) MsCl, NEt_3; 2) 1-Boc-piperazine, KI; iv) 1) TFA/TfOH; 2) Boc_2O, NEt_3.

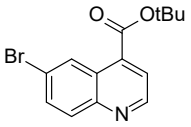

tert-butyl 6-bromoquinoline-4-carboxylate

98.3 mg (390 µmol) 6-bromoquinolie-4-carboxylic acid (raw) were suspended in 5 mL tetrahydrofuran and 25.0 µL (18.3 mg; 181 µmol) triethylamine and added to *O*-tert-butyl-*N*,*N*'-dicyclohexylisourea (prepared the day before from neat 426 mg (2.07 mmol) dicyclohexylcarbodiimide, 173 mg (2.33 mmol) tert-butanol and 10.2 mg (103 µmol) copper(I)iodide). The mixture was heated to 50 °C over night. The mixture was filtered, solvents evaporated and the product isolated by HPLC. 49.7 mg (161 µmol; 41%) of the title compound were obtained after freeze drying.

LC-MS R_t 20.40 min, m/z 251.9642 $[M\text{-}t\text{Bu}]^+$

tert-butyl 6-(4-chlorobutyl)quinoline-4-carboxylate

6.12 mg (19.9 µmol) *tert*-butyl 6-bromoquinoline-4-carboxylate, 1.81 mg (1.98 µmol) $Pd_2(dba)_3$ and 1.85 mg (4.50 µmol) S-Phos were dissolved in 1 mL dry tetrahydrofurane under an inert atmosphere. 200 µL (100 µmol) of a 0.5 M 4-chlorobutyl-1-zinc bromide solution in tetrahydrofurane were added and the reaction was stirred over night. The reaction was quenched with 500 µL of saturated ammonium chloride solution, both phases evaporated and taken up in water acetonitrile 1:1. The mixture was filtered by an oasiss C18 light column before HPLC. 5.82 mg (18.2 µmol; 91%) were obtained after freeze drying.

LC-MS R_t 18.83 min, m/z 320.1393 $[M+H]^+$

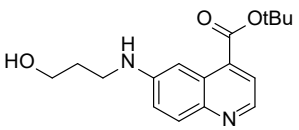

tert-butyl 6-(3-hydroxypropylamino)quinoline-4-carboxylate

6.14 mg (19.9 µmol) *tert*-butyl 6-bromoquinoline-4-carboxylate, 2.56 mg (4.11 µmol) BINAP, 1.61 mg (1.76 µmol) $Pd_2(dba)_3$ and 37.0 (113 µmol) cesium carbonate were dissolved in 1 mL toluene and 5.00 µL (4.95 mg; 65.9 µmol) 1,3-propanolamine were added. The mixture was stirred at 90 °C over night before solvents were removed, the residue suspended in water/acetonitrile 1:1 and filtered before HPLC-purification. 4.41 mg (14.6 µmol; 73%) of the title compound were obtained after freeze drying.

LC-MS R_t 12.95 min, m/z 303.1685 $[M+H]^+$

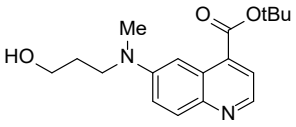

tert-butyl 6-(3-hydroxypropylmethylamino)quinoline-4-carboxylate

99.14 mg (322 µmol) *tert*-butyl 6-bromoquinoline-4-carboxylate, 12.26 mg (19.7 µmol) BINAP, 7.46 mg (8.14 µmol) $Pd_2(dba)_3$ and 212.85 mg (653 µmol) cesium carbonate were dissolved in 3 mL toluene and 64.0 µL (58.9 mg; 660 µmol) *N*-methyl-1,3-propanolamine were added. The mixture was stirred at 90 °C over night before solvents were removed, the residue suspended in water/acetonitrile 1:1 and filtered before HPLC-purification. 62.8 mg (199 µmol; 62%) of the title compound were obtained after freeze drying.

LC-MS R_t 13.41 min, m/z 261.1213 $[M-t\text{Bu}+H]^+$

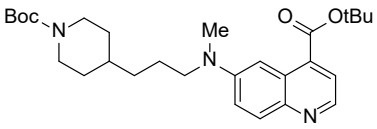

tert-butyl 6-(3-(1-Boc-piperidin-4-yl)propyl-1-(methyl)amino)quinoline-4-carboxylate

3.12 mg (6.45 µmol; 29%) were obtained following the previous method.

LC-MS R_t 19.04 min, m/z 484.3124 $[M+H]^+$

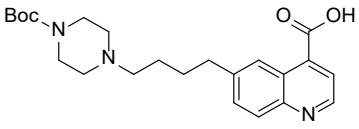

6-(4-(4-*tert*-butoxypiperazin-1-yl)butyl)quinoline-4-carboxylic acid

4.75 mg (14.8 µmol) *tert*-butyl 6-(4-chlorobutyl)quinoline-4-carboxylate were dissolved in 200 µL trifluoroacetic acid (with 2.5% water) and shaken for 180 minutes. 1 mL dichloromethane was added and the solvents removed in vacuo, which was repeated three times. 500 µL dimethylformamide, 35.2 mg (108 µmol) cesium carbonate, 52.41 mg (282 µmol) 1-Boc-piperazine and 7.22 mg (43.5 µmol) potassium iodide were added to the residue. The mixture was shaken at 60 °C over night and purified by HPLC. 3.02 mg (7.29 µmol; 49%) were obtained after freeze drying.

LC-MS R_t 10.78 min, m/z 414.2364 $[M+H]^+$

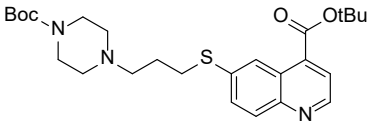

tert-butyl 6-(3-4-*tert*-butoxycarbonylpiperazin-1-ylpropyl-1-thio)quinoline-4-carboxylate

6.35 mg (20.6 µmol) *tert*-butyl 6-bromoquinoline-4-carboxylate, 2.95 mg (4.74 µmol) BINAP, 1.49 mg (1.53 µmol) $Pd_2(dba)_3$ and 36.1 (111 µmol) cesium carbonate were dissolved in 2 mL toluene and 14.78 mg (48.9 µmol) 3-(4-Boc-piperazin-1-yl)-1-(acetylthio)propane were added. The mixture was stirred at 90 °C over night before solvents were removed, the residue suspended in water/acetonitrile 1:1 and filtered before HPLC-purification. 7.82 mg (16.0 µmol; 78%) of the title compound were obtained after freeze drying.

LC-MS R_t 15.96 min, m/z 488.2550 $[M+H]^+$

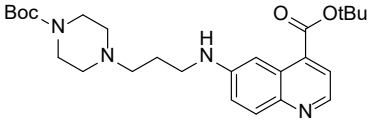

tert-butyl 6-(3-(4-Boc-piperazin-1-yl)propyl-1-amino)quinoline-4-carboxylate

2.39 mg (7.91 µmol) *tert*-butyl 6-(3-hydroxypropylamino)quinoline-4-carboxylate were dissolved in 1 mL dichloromethane and 5.5 µL (4.02 mg; 39.8 µmol) DIPEA. 1.00 µL (1.48 mg; 12.9 µmol) methanesulfonyl chloride were added and the mixture shaken for 60 min. 53.42 mg (28.7 µmol) 1-Boc-piperazine were added before volatiles were removed. 500 µL dimethylformamide and 19.22 mg (116 µmol) potassium iodide were added to the residue. The mixture was shaken at 60 °C for 120 minutes before the product was isolated by HPLC. 3.34 mg (7.09 µmol; 90%) of the title compound were obtained after freeze drying.

LC-MS R_t 13.54 min, m/z 471.2942 $[M+H]^+$

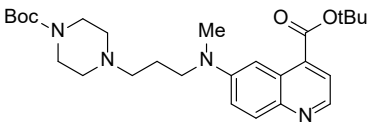

tert-butyl 6-(3-(4-Boc-piperazin-1-yl)propyl-1-(methyl)amino)quinoline-4-carboxylate

62.8 mg (199 µmol) *tert*-butyl 6-(3-hydroxypropylmethylamino)quinoline-4-carboxylate were dissolved in 5 mL dichloromethane and 90.0 µL (66.6 mg; 659 µmol) triethylamine. 20.0 µL (29.6 mg; 258 µmol) methanesulfonyl chloride were added at 0 °C and the mixture reacted for 60 min. 194.6 mg (1.05 mmol) 1-Boc-piperazine were added before volatiles were removed. 500 µL dimethylformamide and 47.4 mg (286 µmol) potassium iodide were added to the residue. The mixture was shaken at 60 °C for 120 minutes before the product was isolated by HPLC. 81.05 mg (167 µmol; 84%) of the title compound were obtained after freeze drying.

LC-MS R_t 13.99 min, m/z 485.3086 $[M+H]^+$

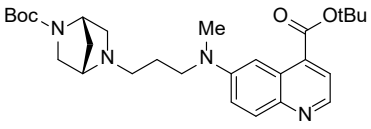

tert-butyl 6-(3-((1*S*,4*S*)-5-Boc-2,5-diazabicyclo[2.2.1]heptan-2-yl)propyl-1-(methyl)amino)quinoline-4-carboxylate

4.05 mg (8.15 µmol; 64%) were obtained following the previous protocol, while the reaction with (1*S*,4*S*)-2-Boc-2,5-diazabicyclo[2.2.1]heptan was carried out at 40 °C over night.

LC-MS R_t 13.79 min, m/z 497.3078 $[M+H]^+$

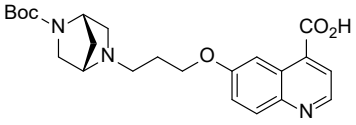

6-(3-((1*S*,4*S*)-5-(*tert*-butoxycarbonyl)-2,5-diazabicyclo[2.2.1]heptan-2-yl)propoxy)quinoline-4-carboxylic acid

3.42 mg (12.9 µmol) of 6-(3-chloro-1-propoxy)quinoline-4-carboxylic acid, 13.3 mg (66.9 µmol) (1*S*,4*S*)-2-Boc-2,5-diazabicyclo[2.2.1]heptan and 18.4 mg (111 µmol) potassium iodide were dissolved in 250 µL DMF. The reaction was shaken at 60 °C over night. The resulting suspension was diluted with 750 µL water before the product was purified by HPLC. After freeze drying 6.46 mg (11.9 µmol; 92%) of the product were obtained as the corresponding TFA-salt.

LC-MS R_t 10.66 min, m/z 450.1768 $[M+Na]^+$

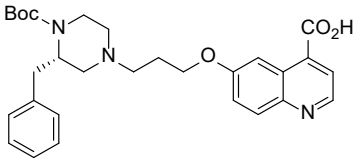

(*S*)-6-(3-(3-benzyl-4-(*tert*-butoxycarbonyl)piperazin-1-yl)propoxy)quinoline-4-carboxylic acid

10.1 mg (16.3 µmol; 85%) were obtained following the previous method.

LC-MS R_t 13.48 min, m/z 506.2388 $[M+H]^+$

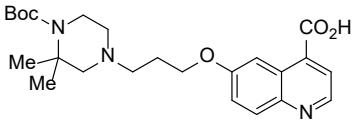

6-(3-(4-(*tert*-butoxycarbonyl)-3,3-dimethylpiperazin-1-yl)propoxy)quinoline-4-carboxylic acid

5.15 mg (9.23 µmol; 46%) were obtained following the previous method.

LC-MS R_t 11.85 min, m/z 444.2260 $[M+H]^+$

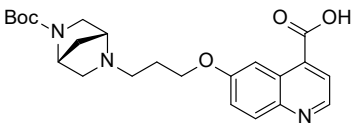

6-(3-((1*R*,4*R*)-5-(*tert*-butoxycarbonyl)-2,5-diazabicyclo[2.2.1]heptan-2-yl)propoxy)quinoline-4-carboxylic acid

2.13 mg (4.98 µmol; 93%) were obtained following the previous method.

LC-MS R_t 10.59 min, m/z 428.2147 $[M+H]^+$

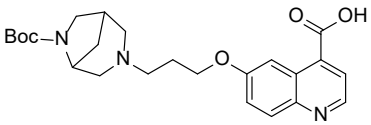

6-(3-(6-(*tert*-butoxycarbonyl)-3,6-diazabicyclo[2.2.1]heptan-2-yl)propoxy)quinoline-4-carboxylic acid

1.59 mg (3.60 µmol; 36%) were obtained following the previous method.

LC-MS R_t 10.92 min, m/z 442.2325 $[M+H]^+$

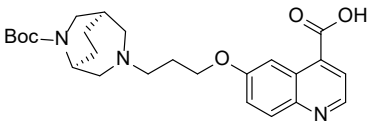

6-(3-((1*R*,5*S*)-6-(*tert*-butoxycarbonyl)-3,6-diazabicyclo[2.2.2]nonan-2-yl)propoxy)quinoline-4-carboxylic acid

3.52 mg (7.73 µmol; 75%) were obtained following the previous method.

LC-MS R_t 11.28 min, m/z 456.2478 $[M+H]^+$

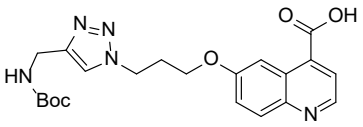

6-(3-(4-(*tert*-butoxycarbonylaminomethyl)-1*H*-1,2,3-triazol-1-yl)propoxy)quinoline-4-carboxylic acid

1.09 mg (4.01 µmol) 6-(3-azidopropoxy)quinoline-4-carboxylic acid were dissolved in 200 µL water and 1 µL (0.86 mg; 15.6 µmol) propargylamine. 1 µL saturated copper(II)acetate in water (0.36 µmol) were added and the solution was heated to 95 °C. The mixture was cooled to room temperature before 50 µL acetonitrile, 4.68 mg (21.5 µmol)

di-*tert*-butyl dicarbonate and 5 µL (3.65 mg; 36.1 µmol) triethylamine were added. The product was isolated by HPLC after 60 min. 1.05 mg (2.45 µmol; 61%) of the title compound were obtained after freeze drying.

LC-MS R_t 12.20 min, m/z 428.1907 $[M+Na]^+$

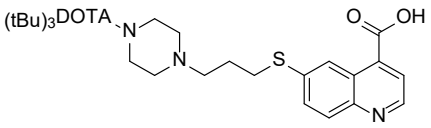

6-(3-(4-(tris-*t*BuDOTA)piperazin-1-yl)propyl-1-thio)quinoline-4-carboxylic acid

4.73 mg (9.69 µmol) *tert*-butyl 6-(3-4-*tert*-butoxycarbonylpiperazin-1-ylpropyl-1-thio)quinoline-4-carboxylate were deprotected with 200 µL trifluoroacetic acid containing 2.5% triethylsilane and 2.5% water for 120 min. The volatiles were removed by coevaporation with dichloromethane (3×1 mL) and the residue dissolved with 100 µL dimethylformamide and 5.50 µL (4.07 mg; 31.6 µmol). Meanwhile 6.89 mg (12.0 µmol) DOTA-tris(*t*Bu)ester and 4.69 mg (12.4 µmol) HBTU were reacted for 10 min in 150 µL dimethylformamide before addition to the deprotected quinoline solution. Finally 10.0 µL (7.40 mg; 57.4 µmol) DIPEA were added and the mixture reacted for 120 min. 6.59 mg (7.44 µmol; 77%) of the title compound were obtained after HPLC-purification and freeze-drying.

LC-MS R_t 13.00 min, m/z 908.4873 $[M+Na]^+$

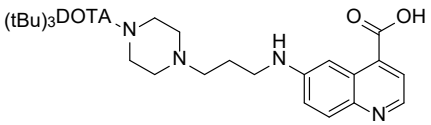

6-(3-(4-(tris-*t*BuDOTA)piperazin-1-yl)propyl-1-amino)quinoline-4-carboxylic acid

1.11 mg (1.28 µmol; 26%) were obtained following the previous protocol.

LC-MS R_t 12.06 min, m/z 891.5258 $[M+Na]^+$

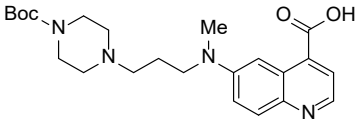

6-(3-(4-Boc-piperazin-1-yl)propyl-1-(methyl)amino)quinoline-4-carboxylic acid

100.12 mg (206 µmol) *tert*-butyl 6-(3-(4-Boc-piperazin-1-yl)propyl-1-(methyl)amino)quinoline-4-carboxylate were treated with 900 µL trifluoroacetic acid, 25 µL triisopropylsilane, 25 µL water and 50 µL trifluoromethanesulfonic acid for 60 min. The deprotected compound was precipitated with diethyl ether, dried and reacted with 60.83 mg (279 µmol) di-*tert*-butyldicarbonate and 50.0 µL (36.5 mg; 361 µmol) triethylamine in 1 mL dimethylformamide for another 60 min. 55.42 mg (129 µmol; 65% over 2 steps) were obtained after HPLC-purification and freeze-drying.

LC-MS R_t 10.52 min, m/z 429.2463 $[M+H]^+$

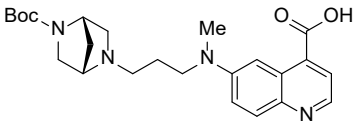

6-(3-((1*S*,4*S*)-5-Boc-2,5-diazabicyclo[2.2.1]heptan-2-yl)propyl-1-(methyl)amino)quinoline-4-carboxylic acid

2.48 mg (5.62 µmol; 88%) were obtained following the previous method.

LC-MS R_t 10.52 min, m/z 441.2464 $[M+H]^+$

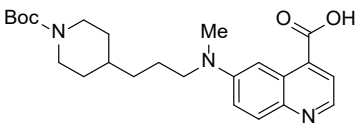

6-(3-(1-Boc-piperidin-4-yl)propyl-1-(methyl)amino)quinoline-4-carboxylic acid

1.57 mg (3.67 µmol; 57%) were obtained following the previous method.

LC-MS R_t 15.51 min, m/z 450.2324 $[M+Na]^+$

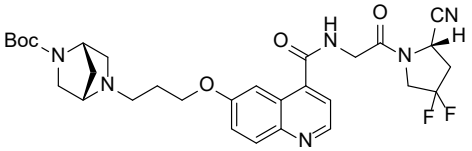

(*S*)-*N*-(2-(2-cyano-4,4-difluoropyrrolidin-1-yl)-2-oxoethyl)-6-(3-((1*S*,4*S*)-5-*tert*-butoxycarbonyl-2,5-diazabicyclo[2.2.1]heptan-2-yl)propoxy)quinoline-4-carboxamide

2.06 mg (5.44 µmol) HBTU in 50 µL DMF were added to a solution of 1.86 mg (4.35 µmol) 6-(3-(4-*tert*-butoxycarbonylpiperazin-1-yl)-1-propoxy)quinoline-4-carboxylic acid, 1.65 mg (12.2 µmol) HOBt and 2.50 µL (1.85 mg; 12.3 µmol) DIPEA in 50 µL DMF. After 15 min 2.26 mg (6.26 µmol) (*S*)-1-(2-aminoacetyl)pyrrolidine-2-carbonitrile 4-methylbenzenesulfonate in 50 µL DMF were added. The reaction was quenched with 500 µL water and purified by HPLC. Freeze drying provided 1.96 mg (3.27 µmol; 75%) of the title compound.

LC-MS R_t 12.41 min, m/z 599.2476 $[M+H]^+$

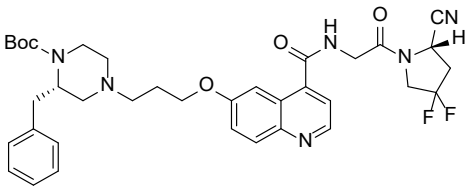

(*S*)-*N*-(2-(2-cyano-4,4-difluoropyrrolidin-1-yl)-2-oxoethyl)-6-(3-(3-(*S*)-benzyl-4-*tert*-butoxycarbonylpiperazin-1-yl)propoxy)quinoline-4-carboxamide

2.54 mg (3.75 µmol; 47%) were obtained following the previous method.

LC-MS R_t 14.83 min, m/z 677.2905 $[M+H]^+$

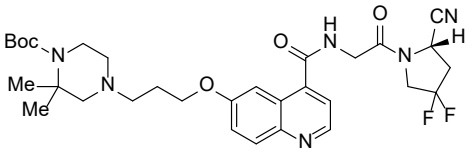

(*S*)-*N*-(2-(2-cyano-4,4-difluoropyrrolidin-1-yl)-2-oxoethyl)-6-(3-(4-(*tert*-butoxycarbonyl)-3,3-dimethylpiperazin-1-yl)propoxy)quinoline-4-carboxamide

2.33 mg (3.79 µmol; 84%) were obtained following the previous method.

LC-MS R_t 13.65 min, m/z 637.2586 $[M+Na]^+$

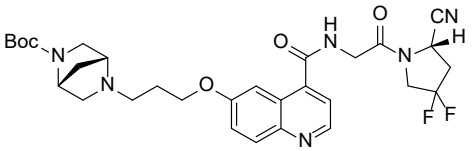

(*S*)-*N*-(2-(2-cyano-4,4-difluoropyrrolidin-1-yl)-2-oxoethyl)-6-(3-((1*R*,4*R*)-5-(*tert*-butoxycarbonyl)-2,5-diazabicyclo[2.2.1]heptan-2-yl)propoxy)quinoline-4-carboxamide

1.58 mg (2.64 µmol; 87%) were obtained following the previous method.

LC-MS R_t 12.44 min, m/z 599.2747 $[M+H]^+$

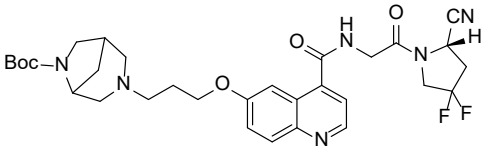

(*S*)-*N*-(2-(2-cyano-4,4-difluoropyrrolidin-1-yl)-2-oxoethyl)-6-(3-(6-(*tert*-butoxycarbonyl)-3,6-diazabicyclo[3.2.1]octan-3-yl)propoxy)quinoline-4-carboxamide

0.57 mg (0.93 µmol; 46%) were obtained following the previous method.

LC-MS R_t 12.59 min, m/z 613.2918 $[M+H]^+$

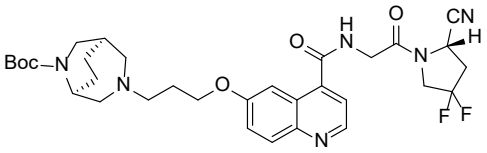

(*S*)-*N*-(2-(2-cyano-4,4-difluoropyrrolidin-1-yl)-2-oxoethyl)-6-(3-((1*R*,5*S*)-6-(*tert*-butoxycarbonyl)-3,6-diazabicyclo[3.2.2]nonan-3-yl)propoxy)quinoline-4-carboxamide

1.22 mg (1.95 µmol; 41%) were obtained following the previous method.

LC-MS R_t 13.08 min, m/z 627.3075 $[M+H]^+$

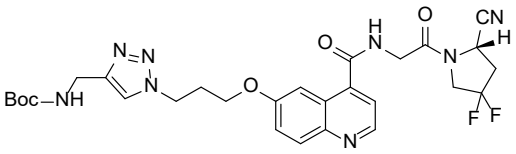

(*S*)-*N*-(2-(2-cyano-4,4-difluoropyrrolidin-1-yl)-2-oxoethyl)-6-(3-(4-(*tert*-butoxycarbonylaminomethyl)-1*H*-1,2,3-triazol-1-yl)propoxy)quinoline-4-carboxamide

0.68 mg (1.14 µmol; 78%) were obtained following the previous method.

LC-MS R_t 13.66 min, m/z 599.2506 $[M+H]^+$

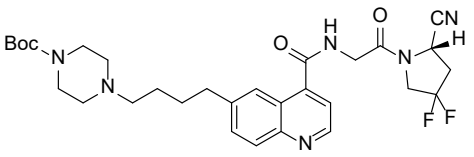

(*S*)-*N*-(2-(2-cyano-4,4-difluoropyrrolidin-1-yl)-2-oxoethyl)-6-(4-(4-(*tert*-butoxycarbonylpiperazin-1-yl)butyl)quinoline-4-carboxamide

3.02 mg (7.29 µmol; 49%) were obtained following the previous method.

LC-MS R_t 13.18 min, m/z 585.2961 $[M+H]^+$

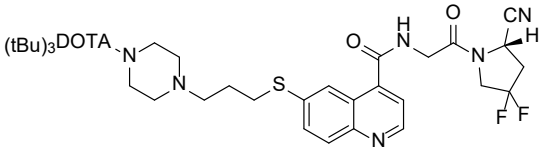

N-(2-(2-cyano-4,4-difluoropyrrolidin-1-yl)-2-oxoethyl)-6-(3-(4-Boc-piperazin-1-yl)propyl-1-thio)quinoline-4-carboxamide

4.91 mg (4.65 µmol; 81%) were obtained following the previous method.

LC-MS R_t 13.78 min, m/z 1079.5466 $[M+Na]^+$

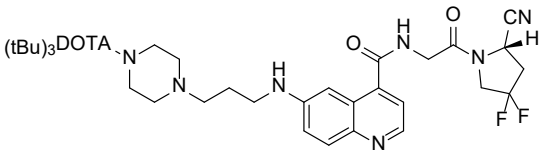

N-(2-(2-cyano-4,4-difluoropyrrolidin-1-yl)-2-oxoethyl)-6-(3-(4-Boc-piperazin-1-yl)propyl-1-amino)quinoline-4-carboxamide

0.74 mg (0.71 µmol; 79%) were obtained following the previous method.

LC-MS R_t 12.89 min, m/z 1062.5860 $[M+H]^+$

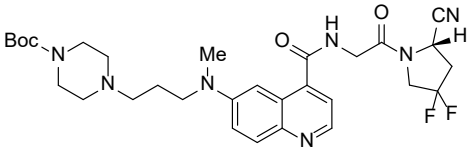

N-(2-(2-cyano-4,4-difluoropyrrolidin-1-yl)-2-oxoethyl)-6-(3-(4-Boc-piperazin-1-yl)propyl-1-(methyl)amino)quinoline-4-carboxamide

0.60 mg (1.0 µmol; 37%) were obtained following the previous method.

LC-MS R_t 12.66 min, m/z 600.3057 $[M+H]^+$

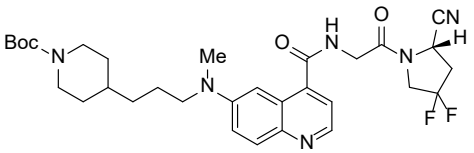

(*S*)-*N*-(2-(2-cyano-4,4-difluoropyrrolidin-1-yl)-2-oxoethyl)-6-(3-(1-Boc-piperidin-4-yl)propyl-1-amino)quinoline-4-carboxamide

51.94 mg (86.6 µmol; 82%) were obtained following the previous method.

LC-MS R_t 16.28 min, m/z 621.2915 $[M+Na]^+$

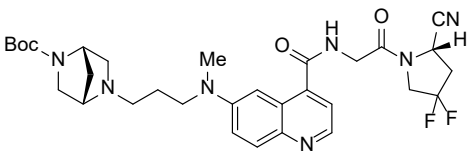

(*S*)-*N*-(2-(2-cyano-4,4-difluoropyrrolidin-1-yl)-2-oxoethyl)-6-(3-((1*S*,4*S*)-5-*tert*-butoxycarbonyl-2,5-diazabicyclo[2.2.1]heptan-2-yl)propyl-1-(methyl)amino)quinoline-4-carboxamide

1.89 mg (3.09 µmol; 78%) were obtained following the previous method.

LC-MS R_t 12.35 min, m/z 612.3062 $[M+H]^+$

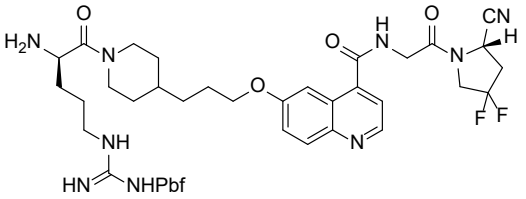

(*S*)-*N*-(2-(2-cyano-4,4-difluoropyrrolidin-1-yl)-2-oxoethyl)-6-(3-(1-D-Arg(Pbf)-piperidin-4-yl)-1-propoxy)quinoline-4-carboxamide

1.11 mg (1.89 µmol) of (*S*)-*N*-(2-(2-cyanopyrrolidin-1-yl)-2-oxoethyl)-6-(3-(1-*tert*-butoxycarbonyl-piperidin-4-yl)-1-propoxy)quinoline-4-carboxamide and 1.87 mg (9.79 µmol) 4-methylbenzene-sulfonic acid monohydrate were dissolved in 50 µL acetonitrile. After 60 min the volatiles removed. To the residue was dissolved in 50 µL dimethylformamide and 2.50 µL (1.85 mg; 14.3 µmol) DIPEA and added to a solution of 2.62 mg (4.04 µmol) Fmoc-D-Arg(Pbf)-OH, 0.61 mg (4.52 µmol) HOBt, 1.70 mg (4.49 µmol) HBTU and 2.50 µL (1.85 mg; 14.3 µmol) DIPEA in 50 µL dimethylformamide. After 60 min 22.2 µL (22.4 mg; 257 µmol) morpholin were added and the product was isolated by HPLC after further 90 min. 1.55 mg (1.73 µmol; 92%) of the title compound were obtained after freeze drying.

LC-MS R_t 14.38 min, m/z 447.7088 $[M+2H]^{2+}$

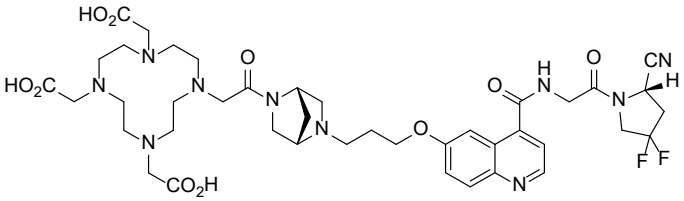

FAPI-21

0.84 mg (1.41 mmol) (*S*)-*N*-(2-(2-cyano-4,4-difluoropyrrolidin-1-yl)-2-oxoethyl)-6-(3-((1*S*,4*S*)-5-Boc-2,5-diazabicyclo[2.2.1]heptan-2-yl)propoxy)quinoline-4-carboxamide were dissolved in 30 µL acetonitrile and 60 µL trifluoroacetic acid. The reaction was shaken for 15 min before volatiles were removed and the residue precipitated by diethyl ether. after centrifugation the solid was taken up in 190 µL dimethylformamide and 5.00 µL (3.65 mg; 36.1 µmol) triethylamine before 1.64 mg (3.12 µmol) of DOTA-*p*-nitrophenol ester were added. The reaction mixture was diluted with 1 mL water and purified by HPLC after shaking for two hours. 0.84 mg (0.95 µmol; 67%) were obtained after freeze drying.

LC-MS R_t 8.90 min, m/z 885.3605 $[M+H]^+$

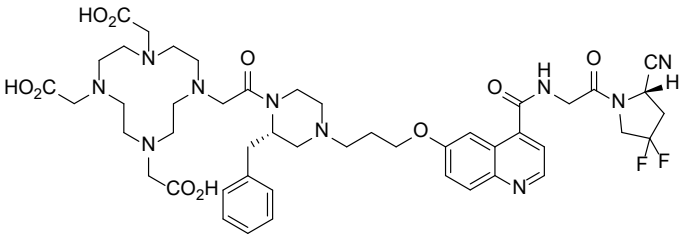

FAPI-22

0.92 mg (0.96 µmol; 67%) were obtained following the previous protocol.

LC-MS R_t 10.18 min, m/z 985.3843 $[M+Na]^+$

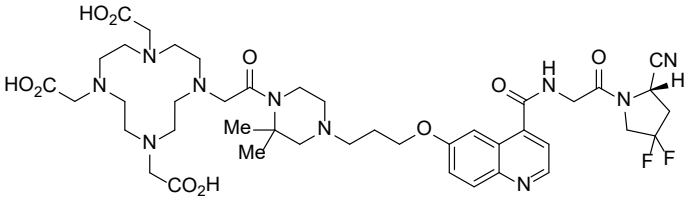

FAPI-23

0.21 mg (0.23 µmol; 14%) were obtained following the previous protocol.

LC-MS R_t 9.13 min, m/z 923.3715 $[M+H]^+$

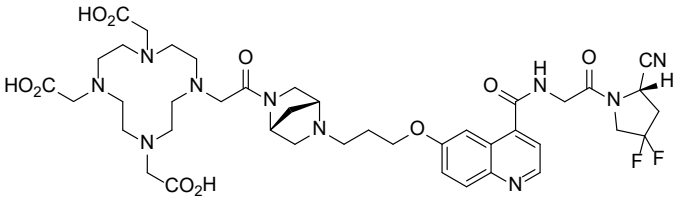

FAPI-31

0.21 mg (0.24 µmol; 14%) were obtained following the previous protocol.

LC-MS R_t 8.92 min, m/z 443.2058 $[M+2H]^{2+}$

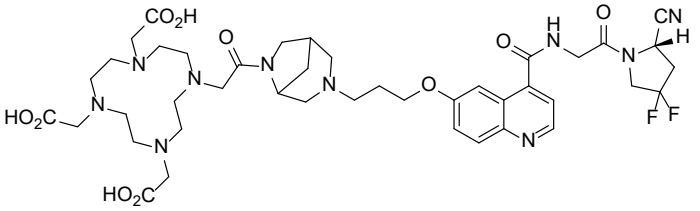

FAPI-35

0.26 mg (0.29 µmol; 71%) were obtained following the previous protocol.

LC-MS R_t 9.26 min, m/z 450.2127 $[M+2H]^{2+}$

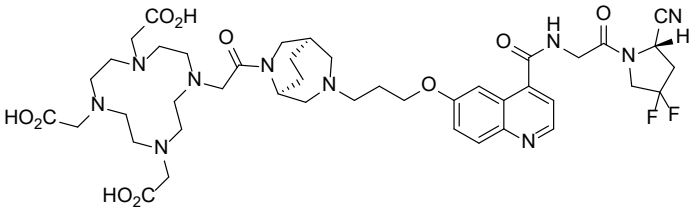

FAPI-36

0.49 mg (0.54 µmol; 96%) were obtained following the previous protocol.

LC-MS R_t 9.36 min, m/z 457.2205 $[M+2H]^{2+}$

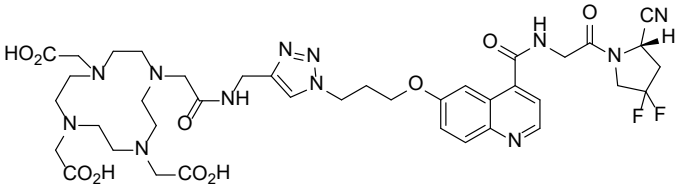

FAPI-37

0.69 mg (0.78 µmol; quant.) were obtained following the previous protocol.

LC-MS R_t 9.66 min, m/z 443.1920 $[M+2H]^{2+}$

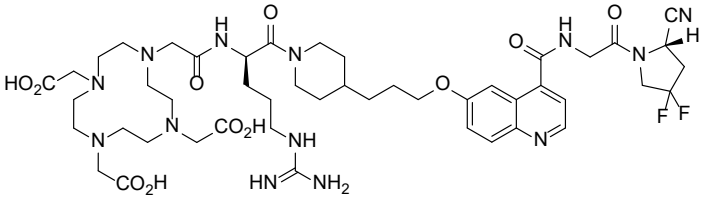

FAPI-38

0.97 mg (0.94 µmol; 78%) were obtained following the previous protocol.

LC-MS R_t 10.46 min, m/z 514.7572 $[M+2H]^{2+}$

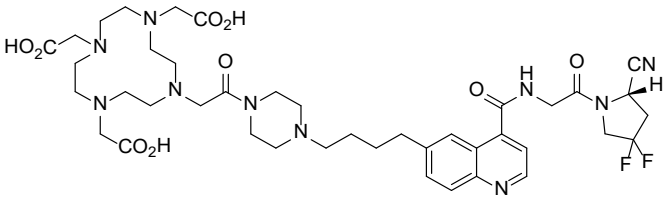

FAPI-39

0.91 mg (1.04 µmol; 71%) were obtained following the previous protocol.

LC-MS R_t 9.19 min, m/z 871.4217 $[M+H]^+$

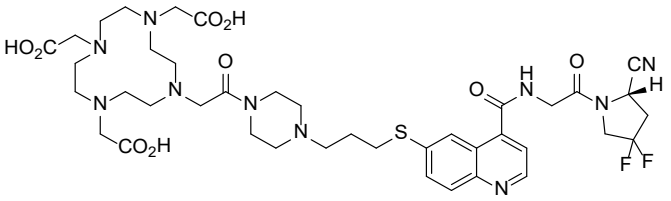

FAPI-40

2.23 mg (2.51 µmol; 69%) were obtained after deprotection with 2.5% trifluorometahesulfonic acid in trifluoroacetic acid/acetonitrile 8:2 for 5 min and HPLC-purification/freeze-drying.

LC-MS R_t 9.63 min, m/z 889.3783 $[M+H]^+$

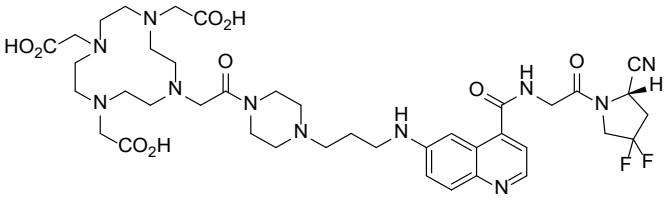

FAPI-41

0.24 mg (0.28 µmol; 74%) were obtained after deprotection with 2.5% trifluorometahesulfonic acid in trifluoroacetic acid/acetonitrile 8:2 for 5 min and HPLC-purification/freeze-drying.

LC-MS R_t 8.56 min, m/z 436.7125 $[M+2H]^{2+}$

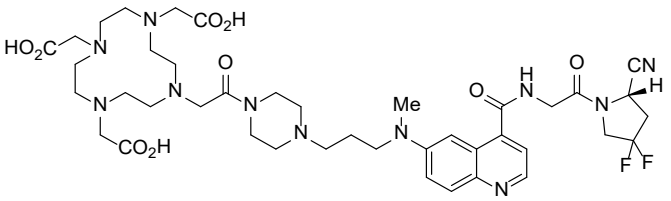

FAPI-46

39.21 mg (44.3 µmol; 85%) were obtained following the procedure for FAPI-21.

LC-MS R_t 9.03 min, m/z 443.7196 $[M+2H]^{2+}$

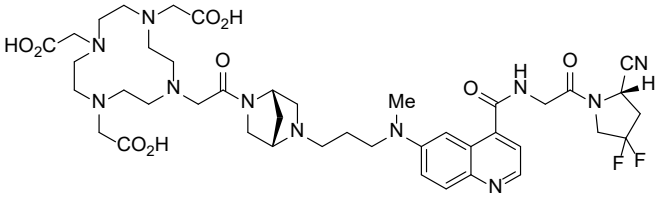

FAPI-53

0.81 mg (0.91 µmol; 41%) were obtained following the previous protocol.

LC-MS R_t 9.09 min, m/z 449.7194 $[M+2H]^{2+}$

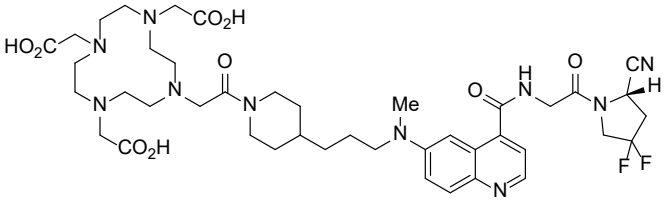

FAPI-55

0.27 mg (0.31 µmol; 63%) were obtained following the previous protocol.

LC-MS R_t 10.78 min, m/z 443.2211 $[M+2H]^{2+}$

Results

Serum stability

Processed and solvent free radioactive compounds (^{177}Lu-FAPI-21 and ^{177}Lu-FAPI-46) were incubated in human sera at 37 °C. After the respective incubation time samples were taken, freed from proteins by precipitation with acetonitrile, centrifuged and the supernatant analyzed via radio-HPLC. Suppl. Figure 1 shows that even at 24 h only the initial (radioactive) peaks are detected and neither radioactive degradation products nor free radioactivity are observed. These findings demonstrate that both substances are unhampered by enzymatic components of human sera.

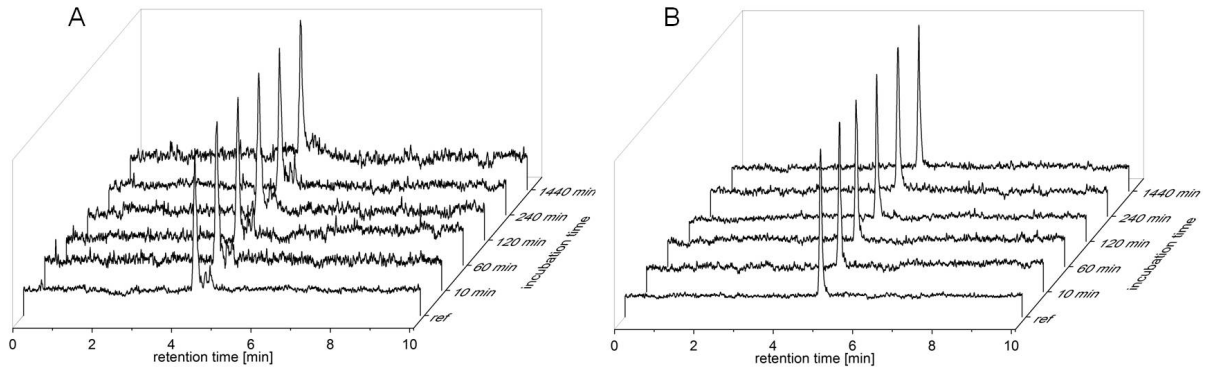

Supplemental Fig. 1. Stability in human serum of A) FAPI-21 and B) FAPI-46.

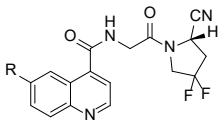

Compound	R-	Compound	R-
FAPI-04	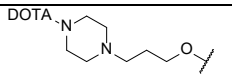	FAPI-37	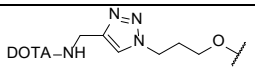
FAPI-20	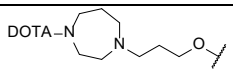	FAPI-38	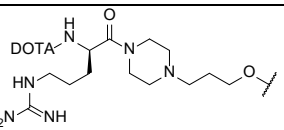
FAPI-21	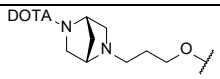	FAPI-39	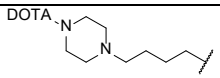
FAPI-22	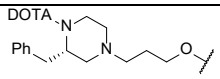	FAPI-40	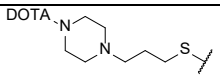
FAPI-23	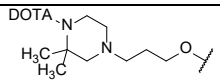	FAPI-41	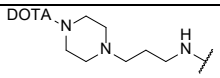
FAPI-31	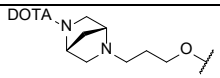	FAPI-46	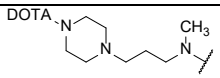
FAPI-35	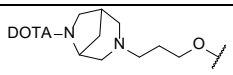	FAPI-53	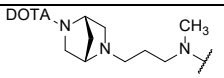
FAPI-36	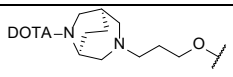	FAPI-55	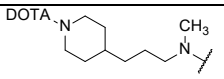

Supplemental Table 1. Chemical structure of the novel FAPI derivatives

In vitro results

	1 h	4 h	24 h
FAPI-04	94,44	94,80	97,09
FAPI-20	97,79	97,75	96,50
FAPI-21	98,04	97,52	97,20
FAPI-22	97,39	96,87	95,16
FAPI-23	95,64	96,45	96,61
FAPI-31	96,35	nd	86,04
FAPI-35	97,03	97,75	95,33
FAPI-36	96,82	96,71	90,13
FAPI-37	97,96	97,40	93,72
FAPI-38	94,77	94,59	63,14
FAPI-39	94,61	94,45	90,90
FAPI-40	95,31	94,92	89,38
FAPI-41	96,81	97,27	83,91
FAPI-46	97,18	97,75	92,03
FAPI-53	93,74	92,97	88,23
FAPI-55	94,60	95,29	94,88

Supplemental Table 2. Percentage of internalized fraction of selected FAPI derivatives in HT-1080-FAP cells after incubation for 1, 4 and 24 h; nd: *not determined*.

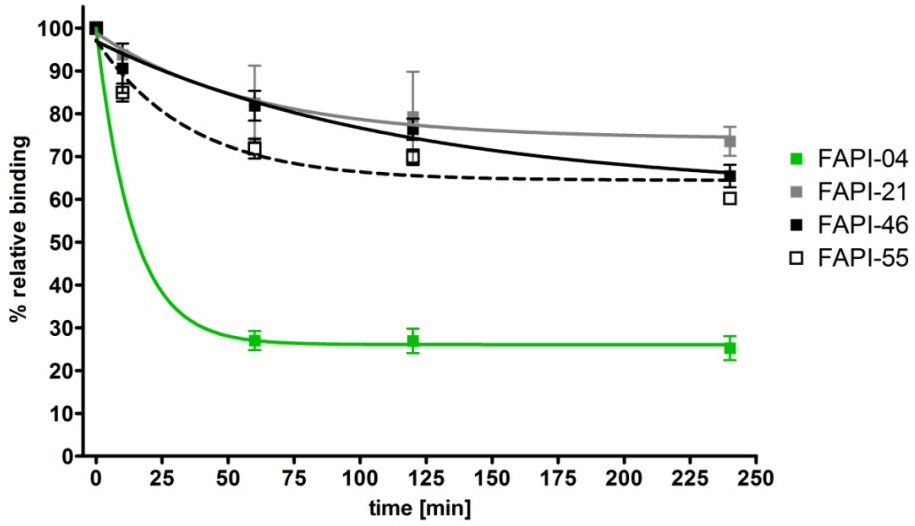

Supplemental Fig. 2. Efflux kinetics of selected FAPI derivatives after incubation of HT-1080-FAP cells with radiolabeled compound for 60 min and consequent incubation with nonradioactive medium for 1 to 4 hours.

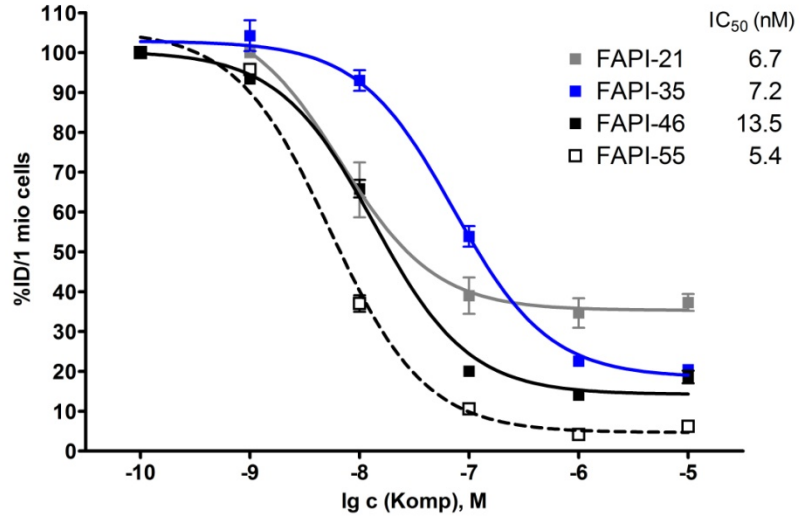

Supplemental Fig. 3. Competitive binding of selected FAPI derivatives to HT-1080-FAP cells after adding increasing concentrations of unlabeled compound.

Small animal imaging

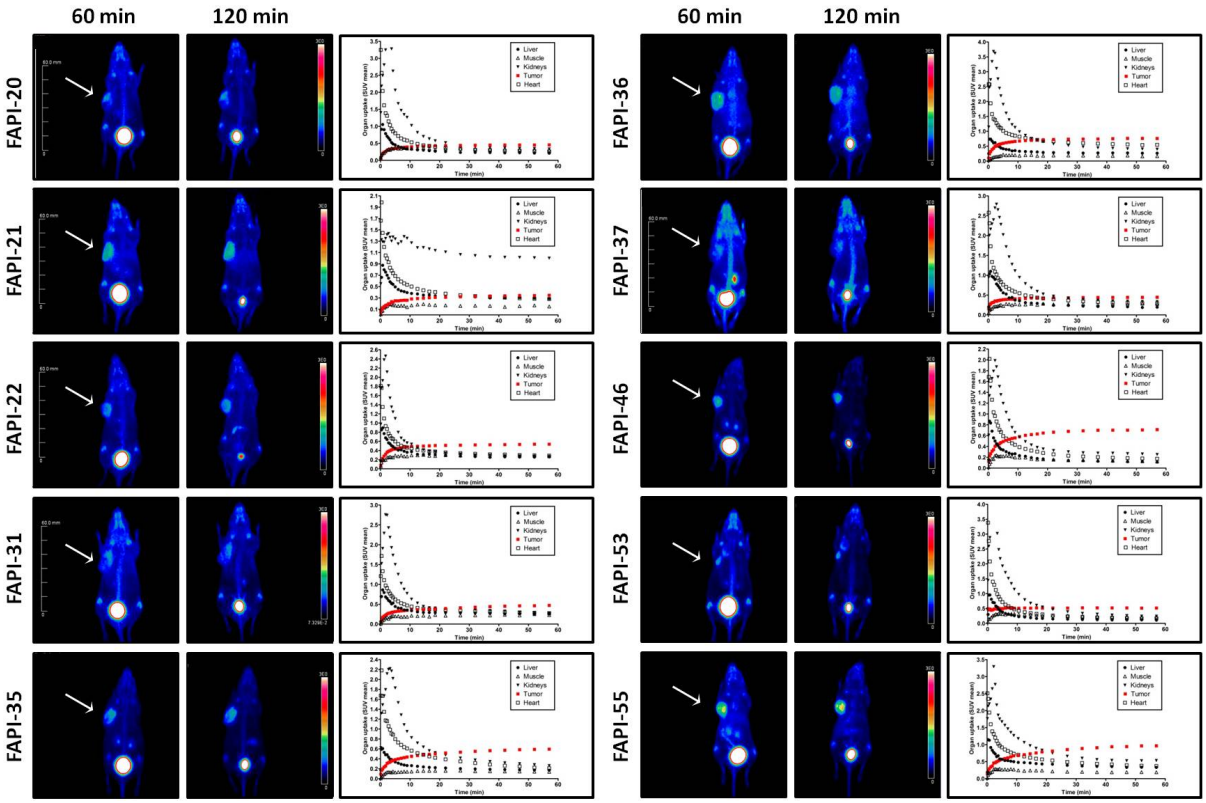

Supplemental Fig. 4. PET imaging of selected FAPI derivatives in HT-1080-FAP tumor bearing mice. Maximum intensity projections (MIP) 60 and 120 min after intravenous injection of ^{68}Ga-labeled compound (tumor indicated by the arrow); time-activity curves up to 60 min after injection.

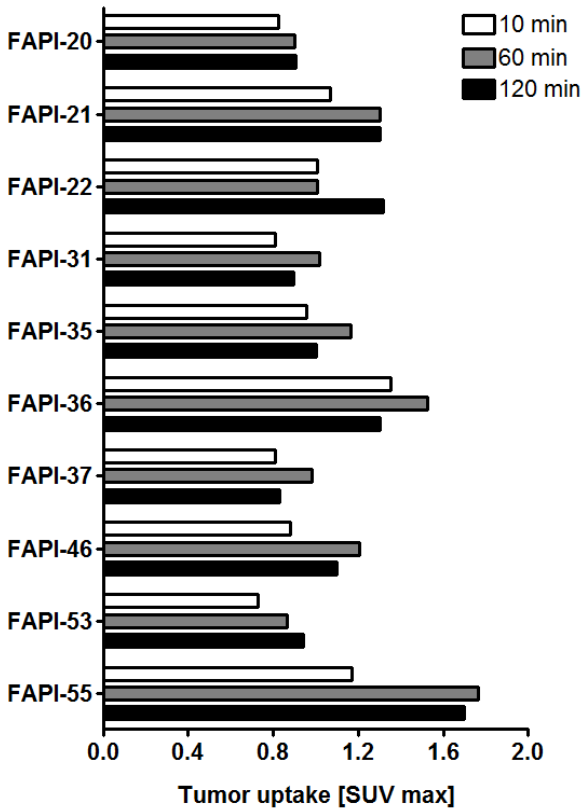

Supplemental Fig. 5. Maximum tumor uptake of ^{68}Ga-labeled FAPI derivatives up to 120 min after intravenous administration, determined by small animal PET imaging.

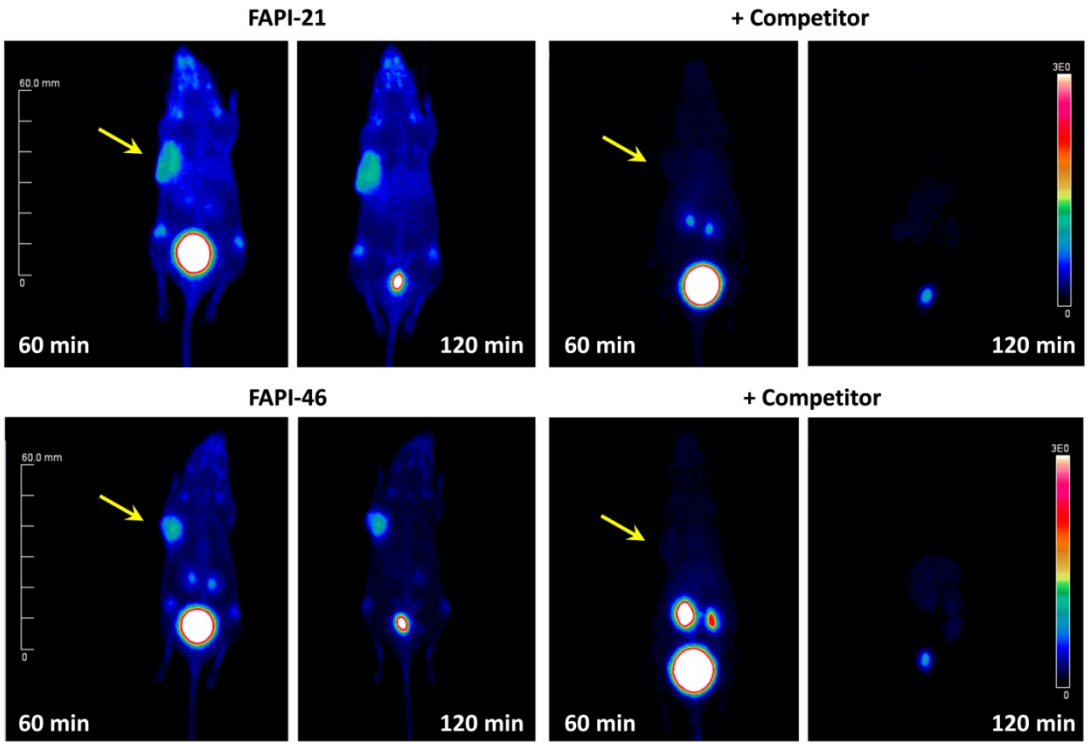

Supplemental Fig. 6. PET imaging of FAPI-21 and -46 in HT-1080-FAP tumor bearing mice. Maximum intensity projections (MIP) 60 and 120 min after intravenous injection of ^{68}Ga-labeled compound (tumor indicated by the arrow) with and without simultaneous administration of unlabeled compound as competitor; n=1.

	Blood	Heart	Lung	Spleen	Liver	Kidney	Muscle	Intestine	Brain
FAPI-04	31.10	48.80	26.33	28.58	17.00	3.35	23.10	43.28	216.26
FAPI-21	29.09	46.52	27.24	26.86	14.37	6.07	21.55	58.15	282.99
FAPI-35	14.32	21.00	13.56	14.55	5.40	2.34	9.55	12.41	167.90
FAPI-46	23.19	40.33	22.66	27.24	19.05	5.40	14.76	38.54	227.41
FAPI-55	12.77	24.35	14.02	30.52	14.15	7.09	10.91	19.87	176.60

Supplemental Table 3. Tumor-to-normal tissue ratios (calculated from %ID/g values 0-24 h after intravenous administration) of ^{177}Lu-labeled FAPI derivatives in HT-1080-FAP tumor bearing mice.

	FAPI-04			FAPI-21			FAPI-46		
	max	**mean**	**n**	**max**	**mean**	**n**	**max**	**mean**	**n**
Tumor	10.07 ± 0.50	5.8 ± 0.3	25	11.93 ± 3.33	5.71 ± 0.61	3	12.76 ± 0.90	6.60 ± 0.53	4
Brain	0.10 ± 0.01	0.86 ± 0.8	25	0.07 ± 0.11	0.01 ± 0.03	4	0.02 ± 0.02	0.00 ± 0.00	4
Oral Mucosa	4.36 ± 0.19	2.50 ± 0.11	25	3.38 ± 1.20	2.39 ± 0.70	4	1.49 ± 1.10	1.29 ± 0.45	4
Parotis	1.58 ± 0.05	1.25 ± 0.04	25	3.69 ± 0.89	2.53 ± 0.33	4	1.38 ± 0.26	1.10 ± 0.34	4
Submandibularis	not determined			7.11 ± 1.24	4.09 ± 0.73	4	2.32 ± 0.75	1.57 ± 0.54	4
Thyroid	2.26 ± 0.11	1.26 ± 0.05	25	3.25 ± 0.89	2.13 ± 0.48	4	2.25 ± 0.46	1.60 ± 0.28	4
Lung	0.68 ± 0.04	0.39 ± 0.03	25	0.92 ± 0.25	0.54 ± 0.13	4	0.99 ± 0.64	0.39 ± 0.19	4
Blood	1.73 ± 0.06	1.08 ± 0.03	25	1.57 ± 0.16	1.14 ± 0.12	4	1.22 ± 0.50	1.11 ± 0.13	4
Liver	1.09 ± 0.05	0.67 ± 0.03	25	1.80 ± 0.26	1.08 ± 0.19	4	1.64 ± 0.48	0.93 ± 0.45	4
Pancreas	1.55 ± 0.08	0.96 ± 0.06	25	3.96 ± 1.34	2.22 ± 0.80	2	1.61 ± 0.55	0.99 ± 0.01	3
Spleen	1.17 ± 0.06	0.76 ± 0.04	25	2.31 ± 0.86	1.24 ± 0.14	3	1.74 ± 0.40	0.92 ± 0.10	4
Kidneys	1.86 ± 0.09	1.38 ± 0.07	25	3.98 ± 0.51	2.40 ± 0.54	4	2.81 ± 0.51	2.02 ± 0.32	4
Muscle	1.54 ± 0.06	1.06 ± 0.04	25	2.41 ± 0.23	1.58 ± 0.23	4	1.80 ± 0.44	1.12 ± 0.29	4

Supplemental Table 4. SUV max and mean values ± standard deviation 1 h after administration of ^{68}Ga-labeled FAPI-04, -21 and -46 to cancer patients; *n: number of patients*. The FAPI-04 data in 25 patients were taken from Giesel, F. *et al.* FAPI-PET/CT: biodistribution and preliminary dosimetry estimate of two DOTA-containing FAP-targeting agents in patients with various cancers. *Journal of nuclear medicine: official publication, Society of Nuclear Medicine*, doi:10.2967/jnumed.118.215913 (2018).